

# Galactic Dynamics without DM Halos or MOND

---

John Herbert Marr<sup>†</sup>

## ABSTRACT

Using Newtonian dynamics and the technique of numerical integration, accurate rotation curves can be derived for any given distribution of disk and bulge mass. It is shown that the stable rotational velocity of a thin disk is highly sensitive to the surface density/mass distribution of the disk, with small changes to the density profiles generating a wide variation in rotational curves, including flat curves. By selecting the bulge mass and disk density distribution with a truncated disk boundary at a defined maximum radius, the models may be fitted to observational data for a range of galaxy types, including low surface brightness (LSB), dense compact galaxies, and bright spirals such as M31. Additionally, conditions consistent with the Tully-Fisher relationship are derived. Although a Newtonian decay might be anticipated at sufficiently remote distances from the galactic centre, the presence of sufficient baryonic matter to make such an observation will continue to influence the rotational velocity of the disk and hence prevent Newtonian decay from being observed; it is therefore postulated that this decay will not be seen. A possible mechanism for the evolution of galactic discs is presented which suggests the emergence of stable flattening rotational curves that approximate to an inverse-r distribution, with the initial disk radius reducing as mass is transferred inwards. A brief thermodynamic analysis also suggests that a galaxy with angular momentum may stabilise for maximum entropy with an inverse-r mass-density disk distribution having uniform velocity. Additional support for galactic dynamics without MOND or DM halos is provided by analysing the evolution and dynamics of an idealised globular cluster such as M15.

---

<sup>†</sup>Marr, JH. *Galactic Dynamics without DM Halos or MOND*. ©2011 Exile Publishing, 1 Armstrong Close, Hundon, Suffolk, UK CO10 8HD. ISBN 978 0 9537917 2 9

*All rights reserved. It is a condition of this publication that it may not be reproduced, quoted, stored in a retrieval system, or transmitted, in any means, whole or in part, by electronic, mechanical, photocopying, recording or otherwise, without acknowledgement of the original title and author. email: [astro@2from.com](mailto:astro@2from.com)*

# Contents

1. INTRODUCTION.....	1
2. THE GRAVITATIONAL ROTATION OF THIN MASSIVE GALACTIC DISKS .....	2
2.1. Background .....	2
2.2. Velocity curves of disks with differing density profiles .....	4
2.3. The gravitational potential within a thin disk of uniform surface density .....	6
2.4. The gravitational force within a thin disk with parametrically decreasing surface density .....	8
2.5. Gravitational force of a thin uniform disk with a central hole.....	12
2.6. The exponential disk.....	14
2.7. The rotational curve for a disk with a Gaussian profile .....	16
2.8. Disks with density profiles as power curves .....	18
2.9. 3-Dimensional disk rotation curves .....	20
2.10. Application of the models to real galaxies .....	22
2.11. NGC 2915.....	22
2.12. M31 .....	23
2.13. NGC 2841.....	24
2.14. Low Surface Brightness (LSB) Galaxies .....	25
2.15. Bright Compact Galaxies – NGC 2683.....	27
2.16. Tully-Fisher relationship.....	28
2.17. Summary of thin disk models.....	32
3. THE EVOLUTION OF GALACTIC DISKS .....	33
3.1. A dynamic model for disk evolution.....	33
3.2. A thermodynamic analysis of the galactic disk .....	36
4. MODEL FOR A SPHERICAL GALAXY .....	37
4.1. Assumptions of the model.....	38
4.2. Equation of motion in a uniform spherical galaxy .....	38
4.3. The IMF and Globular Clusters. ....	44
4.4. The core of globular clusters.....	45
5. CROSS-SECTIONAL DENSITY.....	45
5.1. Sphere with uniform density.....	45
5.2. Sphere with density increasing towards the centre .....	45
5.3. Limitations of the model.....	47
6. DISCUSSION.....	50
7. REFERENCES.....	52

# 1. INTRODUCTION

The observations of flat rotation curves in disk galaxies first reported by Rubin have created a number of problems in their interpretation. Treating the disk as a spherical Newtonian mass generates a simple decay curve which does not agree with the observations. This has led many observers to postulate the existence of a dark matter halo, whose properties conspire with baryonic matter to produce flat rotation curves. A number of DM candidates have some theoretical justification, and their existence may explain other observational data. However, the lack of a good rationale to underpin the theoretical DM density distribution, and the inability of experimentalists to discover any evidence for suitable DM particles, finally led other observers to postulate that Newtonian gravity is incomplete, with the gravitational constant varying at weak field strengths to produce the observed rotation curves (the MOND<sup>1</sup> hypothesis). Although MOND can be adjusted to fit the observed curves well, this *ad hoc* adjustment lacks a credible theoretical justification.

This paper examines the gravitational properties of a number of disk models. It is shown that, far from producing a simple Newtonian decay curve, the stable rotational velocity of a thin disk is highly sensitive to the surface density/mass distribution of the disk, with small changes to the density profiles generating a wide variation in rotational curves, including flat curves. Using only the bulge mass and a disk density distribution with a truncated disk boundary, the models are fitted to the observational data for a range of galaxy types, including low surface brightness (LSB), dense compact galaxies, and bright spirals such as M31. The density distributions used in the models conform well to experimentally observed surface brightness profiles using exponential or inverse- $r$  mass/density functions, while also obeying the Tully-Fisher relationship, and without recourse to DM halos or MOND. Although it might be anticipated that a Newtonian decay will occur at sufficiently remote distances from the galactic centre, this will require the presence of baryonic matter in some form to make the observation. However, this same matter will continue to influence the rotational velocity of the disk and hence prevent Newtonian decay from being observed; it is therefore postulated that this decay will not be seen.

A possible mechanism through which galactic discs evolve is also presented. A stable version of this model predicts the emergence of a flattening rotational curve with the disk radius gradually reducing with time as mass is transferred inwards, leaving a stable mass/density form that approximates to an inverse- $r$  distribution. A variant to this demonstrates a disk instability whereby the outer part of the disk is lost, but this again results in the remaining mass migrating towards the centre, with a truncated edge. Thermodynamic analysis also suggests that a galaxy with angular momentum may stabilise for maximum entropy with an inverse- $r$  mass-density disk distribution having uniform velocity.

Additionally, a model is generated for the evolution of an idealised spherical galaxy or globular cluster from the epoch of galactic separation until it attains stability as a spherical galaxy. It is demonstrated that the ratio of mean separation distance:galactic radius is a constant for a given epoch, with a plausible present day value. Velocity distribution profiles for the globular cluster M15 are also computed, and again, although a mass contribution from DM cannot be excluded, this should mimic baryonic matter, and the theoretical curves may be fitted to observational values without MOND.

## 2. THE GRAVITATIONAL ROTATION OF THIN MASSIVE GALACTIC DISKS

The motion of a test mass in the field of a thin, massive gravitational disk differs significantly from its behaviour in a uniform sphere of matter, and is exquisitely sensitive to the surface density profile of the disk. Additionally, it is shown that there is a profound change in the gravitational field profile and corresponding rotational velocity curve, dependent on whether the disk has an abrupt or tapering termination. A number of disk profile models are described, and it is demonstrated that variations in the disk surface density profile can mimic the observed rotational velocities for a number of “typical” disk galaxies with a plausible range of masses, while obeying the Tully-Fisher relationship. Specifically, disks with an exponential surface density profile and an abrupt cut-off closely mimic a range of low surface brightness (LSB) galaxies, while those with an inverse- $r$  surface density profile closely mimic the flat rotational curves of bright dense galaxies. These close fits to observations are possible within a strictly classical Newtonian model, without the requirement for a dark matter halo or a variable gravity model.

### 2.1. Background

The gravitational potential and resultant motion of a point test mass within a model galaxy is a complex function of the mass distribution within the galaxy. Unlike the gravitational potential within and external to a uniform massive sphere, that within a disk of matter does not yield to simple analytical methods of integration but requires numerical methods for its solution. Galactic models using spherical symmetry suggest an increase in the rotational velocity proportional to radius on moving from the centre towards the edge of the bulge, then an asymptotic decrease in rotational velocity proportional to  $r^{-1/2}$  when moving away from and external to the bulk mass. The failure of the observed rotational velocity curves of galaxies to fit this simplistic model has supported the postulate for dark matter, distributed in such a way as to balance the equations to generate a flat velocity curve. Because dark matter has not been observed at the present time, subsequent attempts to explain the failure have suggested a breakdown of Newton’s laws in regions of low gravity, and introduced the concept of a variable gravity, or MOND model<sup>1</sup>. Advocates of MOND, including Sanders<sup>2,3</sup> Swaters<sup>4</sup> and de Blok<sup>5</sup>, support the idea that dynamics or gravity is non-Newtonian in the limit of low accelerations and that it is unnecessary to invoke the presence of large quantities of unseen matter. Other attempts to describe galactic dynamics without recourse to dark matter include the application of a modified acceleration law obtained from Einstein gravity coupled to a massive skew-symmetric field<sup>6</sup>; general relativistic attempts to explain flat galactic rotation curves<sup>7</sup>; and a logarithmic correction to the Newtonian field<sup>8</sup>.

In this paper, the gravitational potential associated with disk galaxies is examined in some detail, and the associated stable rotational curves are presented. It is demonstrated that the potential, and hence the velocity profile, is highly dependent on the surface density profile of the disk, and a large range of velocity curves can be generated from a few basic disk parameters. Although dark matter may exist within the disk profile, it is sufficient that the gravitational distribution of the dark matter mass follows the observed distribution of baryonic mass. Specifically, there is no requirement to invoke an independent dark matter halo, nor to resort to a variable gravitational constant or changes in Newton’s gravitational laws to generate a flat rotational curve. It is demonstrated that the velocity curves do not vary greatly when a thick disk is substituted for an ideal thin disk, and these curves also obey the Tully-Fisher law for a number of profiles.

Historically, a number of papers have discussed the analysis of velocity rotational curves of thin disk galaxies as a function of the surface density. Eckhardt and Pestaña<sup>9</sup> presented a technique for calculating the midplane gravitational potential of a thin axisymmetric galactic disk. They derived a number of mathematical expressions for assessing the compatibility of observed brightness and Doppler distributions of galactic disks, and for testing a number of gravitational theories, using the power of Wolfram Mathematica to compute the derived functions. Simple methods of numerical integration have been presented by Nicholson<sup>10</sup> and Banhatti<sup>11</sup>; Kochanek<sup>12</sup> has described an integration method for equatorial rotation curves, and more recently Keepports<sup>13</sup> has demonstrated the construction and evaluation of an integral for the gravitational field for an idealized planar galaxy with circular symmetry as a function of radial distance.

Analytical techniques suffer from four major problems: 1) The mathematical analysis is complex, and they can only be used with simple assumptions about the surface density distribution; 2) They often suffer from an infinity problem as the radial integration crosses the radial position of the test mass, sometimes solved by placing the test mass off centre from the galactic disk; 3) They generally have to extend the galactic radius to infinity, which demands an exponentially decreasing surface density; 4) They are unable to cope with a finite boundary. This paper approaches the problem from the perspective of deriving rotational curves from any given surface density distribution. By using numerical integration rather than an analytical technique, it is relatively easy to derive these curves for any density distribution, including boundary conditions at a finite  $R_{max}$ , and – though not considered here - any arbitrary gravitational law. The infinity problem is also easily solved by programmatically handling division by zero errors.

The inverse problem – the derivation of galactic disk surface density profiles from the observed rotational curves – is computationally difficult. Given the velocity curve, Toomre<sup>14</sup> derived a theoretical function to obtain the mass density distribution to produce the curve, and illustrated this with a number of examples limited only by the availability of appropriate mathematical analytical functions. Although he stressed that no unique advantages could be claimed for these models except that both their rotation and density laws could be exactly expressible in terms of relatively simple functions, he nevertheless concluded that these rotation profiles were not unlike some that are observed. This approach has been further developed by Freeman<sup>15</sup>, Kent<sup>16</sup>, Cuddeford<sup>17</sup>, and Conway<sup>18</sup>. Although this form of calculation is valuable in deriving a density distribution from an observed velocity curve, the oscillatory behaviour of the Bessel functions makes the integration difficult except for special solution families.

The first section of this paper looks at a number of self gravitational disk models, with differing parameters for the disk profile, with and without a central bulge mass. Varying the disk thickness with uniform density is mathematically identical to varying the surface density of a thin disk, and it is shown that by varying the assumed disk profile, a wide range of disk galaxy types can be mimicked, with differing velocity curves which are sensitive to the density profile chosen for the model. Three principle profiles emerge from this analysis: Type 1, in which the velocity curve continues to rise with no maximum, and no flat portion; Type 2, which rises to a maximum  $v_{max}$  before falling away; and Type 3, which is an infection curve with a flat plateau,  $v_{flat}$  then a terminal rise. These curves are similar to the observational velocity profiles reported for a number of galaxies, and broadly correspond to the three galaxy profiles described by Verheijen<sup>19</sup>. In particular, it is noted that a surface density profile that has an inverse-r relationship is associated with a flat rotational curve over much of the radial parameter.

The second section looks at how finite disk thickness might influence the model curves for uniform and inverse- $r$  surface density profiles.

The third section examines the application of the modelling technique to fitting the published rotation curves for a number of galaxies. It is demonstrated that a number of these galaxies will fit a model having an exponential surface density with a sharp finite cutoff with or without a bulge, while others require an inverse- $r$  surface density, usually with a massive bulge.

The final section confirms that a specific class of exponential disks and the inverse- $r$  disks both fulfil the Tully-Fisher relationship.

## 2.2. Velocity curves of disks with differing density profiles

As a prelude to looking at realistic galactic disks, this section examines the gravitational force acting on a test particle within disks of matter with various cross-sectional profiles, with and without a central mass. The first model examined is a disk with uniform density  $\Sigma_0$  (and hence thickness  $\delta h$ ), with unit mass per unit area, and having unit radius; such a disk has a total mass of  $\pi$ . In subsequent models, the density profiles are functions of the disk radius; mathematically, these are equivalent to a disk of uniform volumetric density, but whose thickness,  $\delta h$ , varies as the radius function.

### 2.2.1. Assumptions of the models

Assumptions made throughout the models are:

- Radial symmetry about the centre.
- Disks have negligible thickness compared with their radii.
- Matter is distributed continuously within the disk, rather than as discrete point masses.
- The motion of the test mass within the disk is a uniform circular motion, whose velocity is sufficient to balance the inward net gravitational force.
- Where a bulge is present, this is assumed to be spherical, and of uniform density.
- The mass of any central black hole is assumed to be negligible compared with the mass of the bulge.
- The effect of any halo mass is minimal and is not examined in these disk models.
- The effect of bars or spiral arms within the disks is not considered.

### 2.2.2. The gravitational potential of an annulus

As a prelude to the fuller analysis of disks of varying density, we introduce the gravitational field in the plane of a massive annulus (Figure 1).

Let  $F$  be the gravitational force acting on a test particle at  $P$  (where  $OP=r$ ) from a thin, narrow, massive ring, radius  $r_j$  centred on  $O$ , width  $\delta r$ , thickness  $\delta h$ , and density  $\rho_0$ .

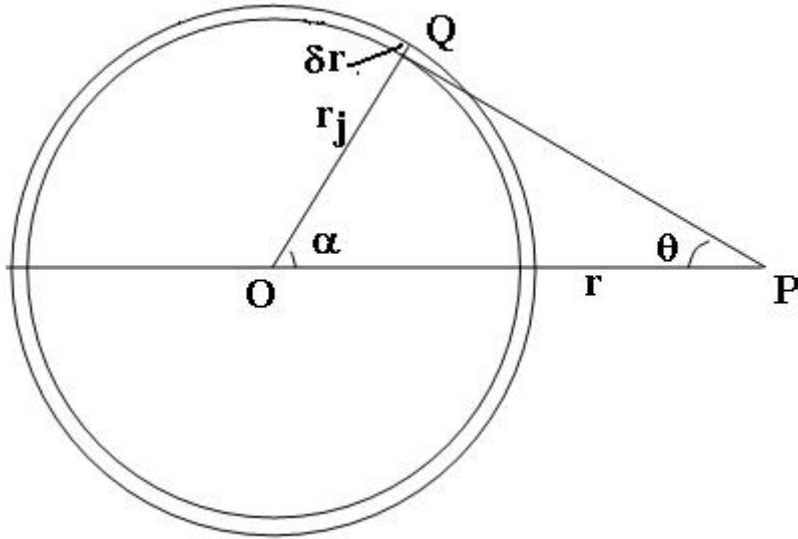


**Figure 1. Gravitational force of a massive annulus**

Consider a small element of the ring of mass  $\delta m$  at  $Q$ , subtending angle  $\delta\alpha$  at centre  $O$  (Figure 1). Then the gravitational attraction of  $\delta m$  on unit mass at  $P$  is:

$$\delta F = \frac{G\delta m}{PQ^2} \quad (2.2.1)$$

The resultant gravitational force  $\delta F_x$ , directed towards  $O$ , and taken to be positive towards the centre, is then:

$$\delta F_x = \frac{G \cos \theta \delta m}{PQ^2} \quad (2.2.2)$$

where

$$\delta m = \rho_0 r_j \delta\alpha \delta r \delta h \quad (2.2.3)$$

$$\cos \theta = \frac{r - r_j \cos \alpha}{PQ} \quad (2.2.4)$$

$$PQ^2 = r^2 + r_j^2 - 2rr_j \cos \alpha \quad (2.2.5)$$

We may ignore  $\delta F_y$  through symmetry, and  $\delta F_z$  is zero for a thin disk. Hence:

$$F_x = \frac{C_1 r_j (r - r_j \cos \alpha) \delta r \delta \alpha}{(r^2 + r_j^2 - 2r_j r \cos \alpha)^{3/2}} \quad (2.2.6)$$

where

$$C_1 = G\Sigma_0 \quad (2.2.7)$$

and  $\Sigma_0 = \rho_0 \delta h$  is defined as a mean surface density. Integrating over the whole ring:

$$F_x = \int_0^{2\pi} \frac{C_1 r_j (r - r_j \cos \alpha) \delta r}{(r^2 + r_j^2 - 2r r_j \cos \alpha)^{3/2}} \delta \alpha \quad (2.2.8)$$

The analytical integral solution is non-trivial, containing components of elliptical integrals of the first and second kind, but this may be solved by computational analysis using the methods of numerical integration. For  $0 \leq r \leq 2$  and taking  $r_j = 1.0$ ,  $C_1 = 1$ , we may plot the gravitational potential on the point mass at  $r$  (Figure 2). As expected, this is asymptotic *w.r.t.* the annulus, being negative within the ring, and positive at points more distal. The asymptote exists because the model takes the annulus to be of infinitesimal thickness, leading to a denominator that approaches zero.

For an annulus of unit density/length, the total mass is  $2\pi$ , and the curve for an equivalent central mass is included for comparison, confirming that the two curves converge asymptotically for  $r \gg 1$ .

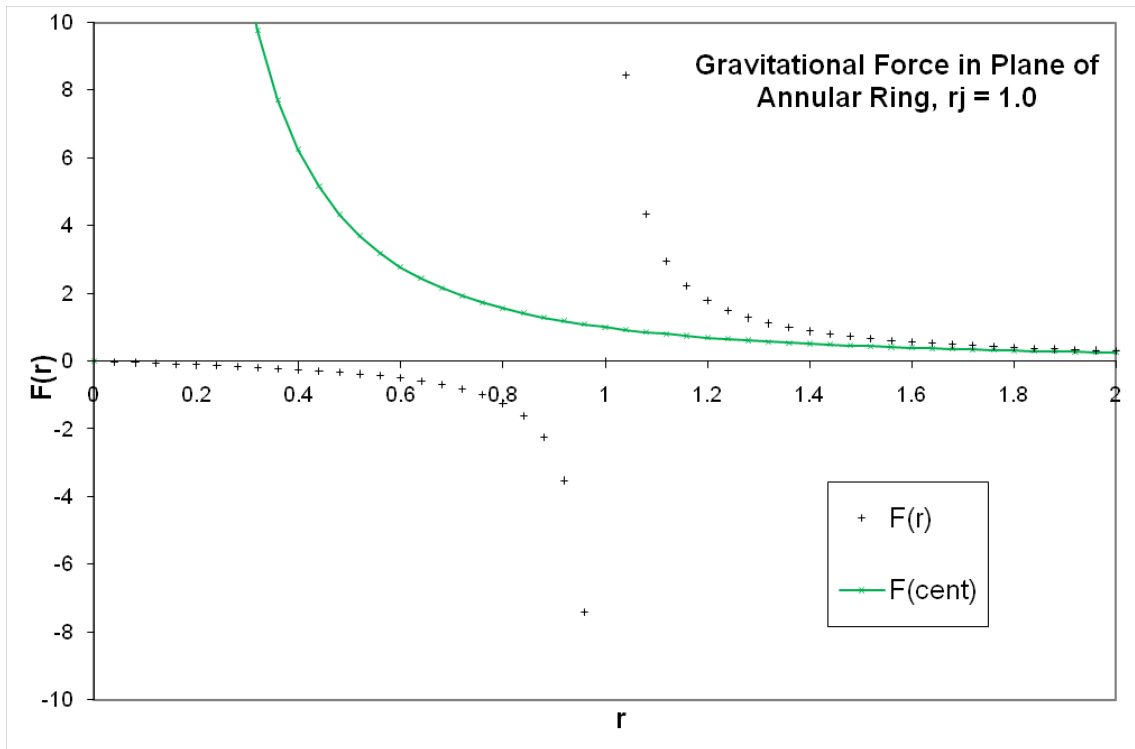
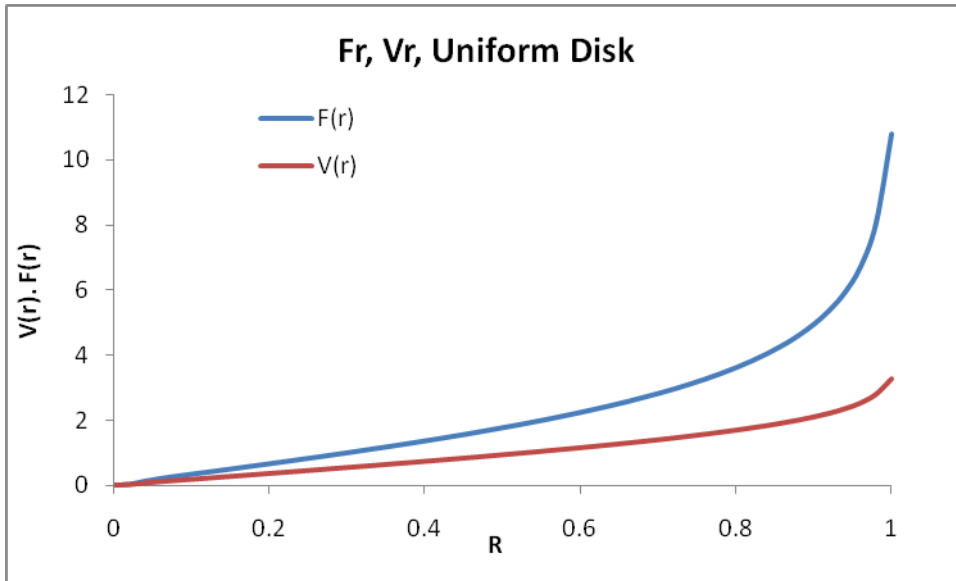


Figure 2. Gravitational force in plane of annulus

### 2.3. The gravitational potential within a thin disk of uniform surface density

A thin disk may be considered as an infinite number of annuli of width  $dr$ , uniform surface density  $\Sigma_0$ , and negligible thickness  $\delta h$ . Letting the disk have unit radius, the total gravitational attraction on a point mass lying within the plane of the disk is given by the double integral (2.3.1). For a point mass at a distance  $r_i$  from the centre, the total gravitational force towards the centre is:

$$F_x = \int_0^1 \int_0^{2\pi} \frac{C_1 r (r_i - r \cos \alpha)}{(r^2 + r_i^2 - 2r r_i \cos \alpha)^{3/2}} d\alpha dr \quad (2.3.1)$$



**Figure 3. Rotational velocity curve for point mass within uniform thin disk of mass  $\pi$**

where  $C_1$  is defined as before. Figure 3 is the plot of  $F_x$  for  $0 \leq r \leq 1$ , using the numerical integration method of the compound mid-point rule<sup>20</sup>. The linear velocity  $V(r)$  for a test mass moving in a stable orbit at equilibrium is also plotted, using the relationship:

$$V(r) = \sqrt{F r} \quad (2.3.2)$$

Unlike the gravitational force and velocity within a massive sphere, the gravitational field and linear velocity for a thin, uniform massive disk increase approximately linearly until approaching  $r = 1$  where a steep change of gradient occurs.

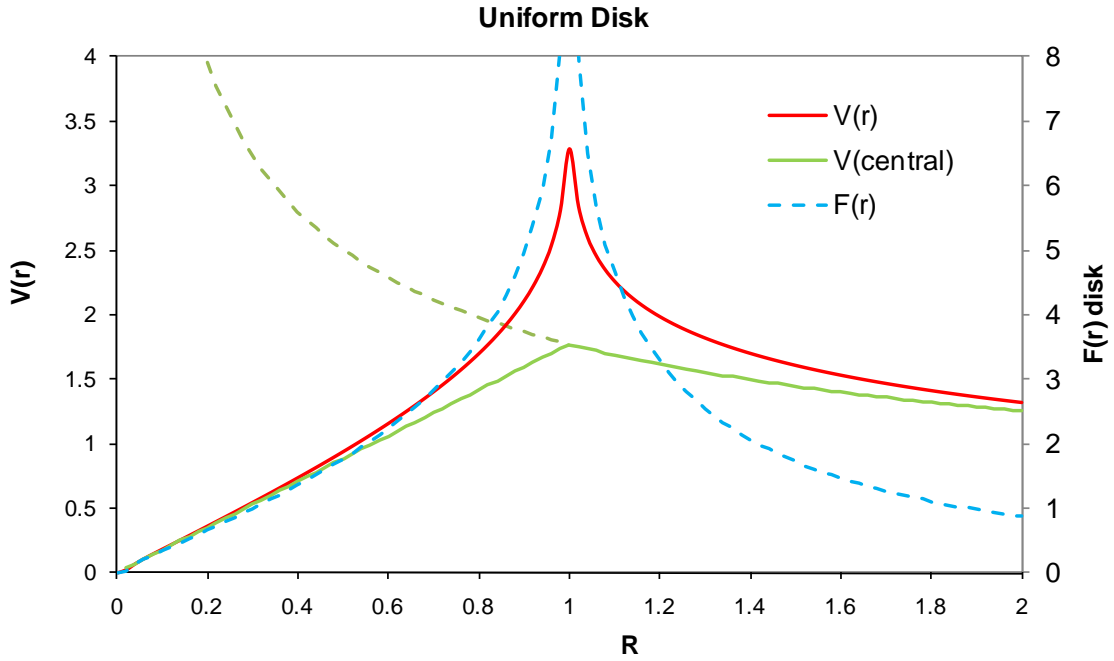


**Figure 4. Rotational velocity curves for uniform disk, sphere, and point mass  $\pi$**

The total mass of the disk is  $\pi$ . However, because of the lack of spherical symmetry, the mass does not act as a point mass beyond the disk edge until  $r \gg I$ . This may be shown by extending  $r$  beyond the edge of the disk (Figure 4) and comparing this with the rotational velocity associated with a central point mass  $\pi$  (dashed green line). The solid green line plots the internal and external rotational velocity associated with an equivalent massive sphere of unit radius and mass  $\pi$ . The accuracy of the numerical integration method employed may be estimated by generating the disk mass within the integration; for increments of  $\delta r = 0.001$ , and  $\delta \alpha = 1^\circ$ ,  $Md = 3.147879$ , equivalent to an accuracy of 0.2% when compared with the theoretical mass of  $\pi$ .

### 2.3.1. Rotational curve Type 1

The characteristic shape of the velocity curve for a uniform disk shown in Figure 3 may be classified as a Type 1 rotational curve. Verheijen<sup>19</sup> has described rotation curves that continue rising until the last measured point as ‘R–curves’. In these cases, the observed maximum rotational velocity is determined by the extent of the HI disk and provides a lower limit to the actual maximum rotational velocity induced by the gravitational potential. This type of rotation curve is often observed in dwarf galaxies and in spirals with an HI disk that is confined to the inner regions<sup>19</sup>.

## 2.4. The gravitational force within a thin disk with parametrically decreasing surface density

Continuing with the simplification that we may take the surface density  $\Sigma$  as the variable with radius for a disk that is very thin compared to its radius, then to a first approximation, a galaxy disk profile may be parameterised with three characteristic

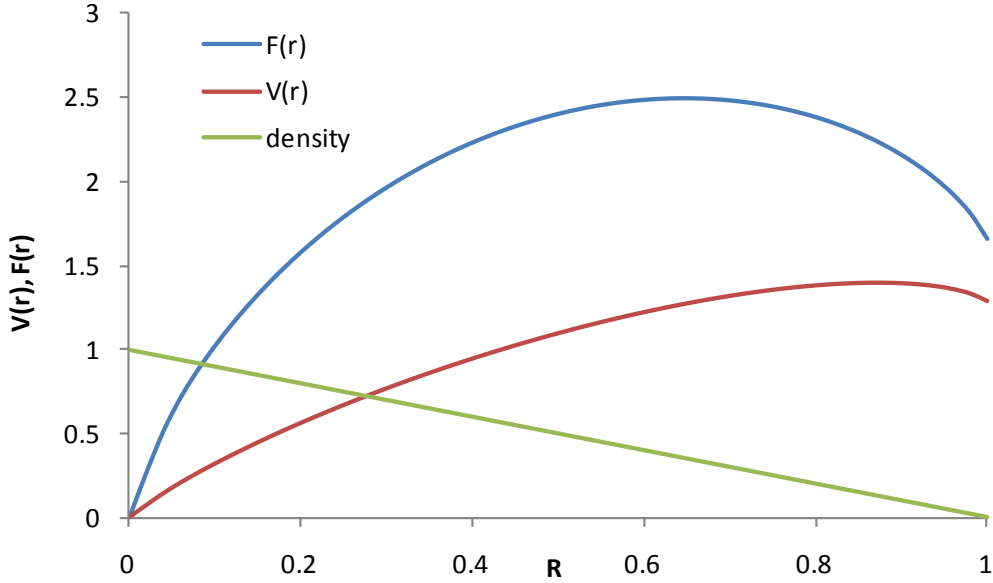


**Figure 5. Velocity curve for point mass within wedge shaped disk**

surface densities,  $\Sigma_0$ ,  $\Sigma_1$ ,  $\Sigma_2$  corresponding to the maximum thickness at  $\mathbf{r}(0)$ ,  $\mathbf{r}(0.5)$  and  $\mathbf{r}(1)$  respectively.

This function may be parameterised as:

$$\Sigma(r) = \Sigma_0 \left( a + \frac{b}{c+r} \right) \quad (2.4.1)$$

Varying the parameters  $\Sigma_1$  and  $\Sigma_2$  is sufficient to produce a wide range of surface density profiles, with a correspondingly wide range of velocity profiles, as considered in the following sections.

#### 2.4.1. The gravitational force within a thin disk with linearly decreasing surface density

For a simple ‘wedge’ disk (Figure 5),  $\Sigma_0=1$ ;  $\Sigma_1=0.5$ ;  $\Sigma_2=0$ . This form corresponds to a density profile of the form:

$$\Sigma(r) = \Sigma_0(1 - r) \quad (2.4.2)$$

(mathematically equivalent to a disk whose profile is a thin linear wedge of uniform density but linearly decreasing thickness,  $\mathbf{h}$ ). The corresponding rotational velocity  $\mathbf{V}(r)$  is plotted in Figure 5.

#### 2.4.2. Rotational curve Type 2

In contrast to the uniform disk model, both the gravitational force and hence velocity  $\mathbf{V}(r)$  of a test particle within the wedge disk have maxima before decreasing towards the periphery of the disk. This characteristic shape for the velocity curve may be termed a Type 2 rotational curve, and is characteristic of a disk whose surface density decreases to

zero at the edge. The density profile of the disk is included, and the total mass of such a disk is  $\pi/3$ . For the Type 2 curve of Figure 5, generated from the theoretical wedge shape shown,  $V(r)_{max} = 1.40$  and  $R_{max} = 0.88$ .

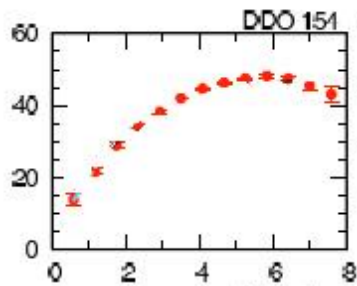


**Figure 6. Rotation curve for DDO154<sup>21</sup>**

Verheijen<sup>19</sup> has described rotation curves which reach a maximum in the optical regions after which they decline to an extended flat part in the outer disk, with the maximum rotation velocity exceeding the amplitude of the flat part ('D-curves'). It should be noted however that, while the shape of the D-curves of Verheijen are computed using an extended dark-matter halo, the Type 2 curves presented in this paper are generated only with matter distributed within the defined disk.

A Type 2 rotation curve is shown for the dwarf galaxy DDO154 (Figure 6) from observations presented by Carignan and Purton<sup>21</sup>. They described the rotation curve obtained as one of the most extended, relative to the optical size of the galaxy, ever derived. It extends 33% further than that obtained from the VLA data alone, and confirmed that the rotation curve is declining in the outer parts.

This behaviour of the rotation curves with  $V_{max} > V_{terminal}$  is often seen in massive early-type spirals and in galaxies with a compact distribution of their luminous matter (e.g. Casertano & Van Gorkom<sup>22</sup>).

### 2.4.3. The gravitational force within a thin disk with non-linearly decreasing surface density

By building an integration model using these three parameters for the galaxy profile (again ignoring the presence of a central bulge and any halo effect), it is possible to generate velocity curves from a range of theoretical galaxy profiles. Figure 7 corresponds to a wedge outline with a compressed waist, here with  $\Sigma_1=0.1$  at  $r(0.5)$  and  $\Sigma_2=0$  at  $r(1)$ ; the velocity curve is now flatter, but again falls from a maximum, and is therefore again a Type 2 rotational curve. The surface density profile of this disk is also presented, and the disk mass is  $M_d \approx 0.08\pi$ .

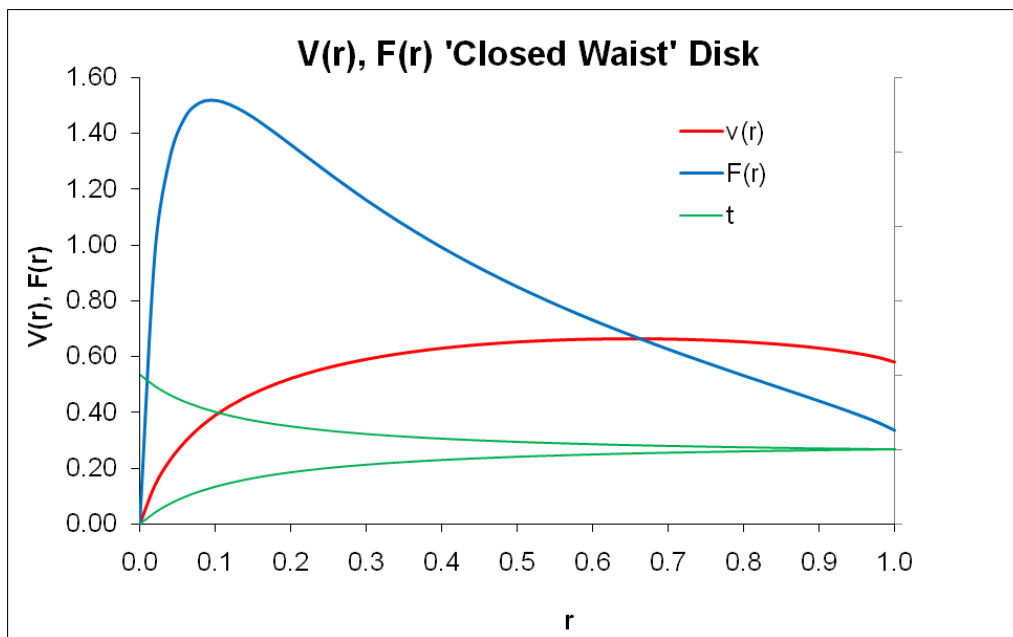
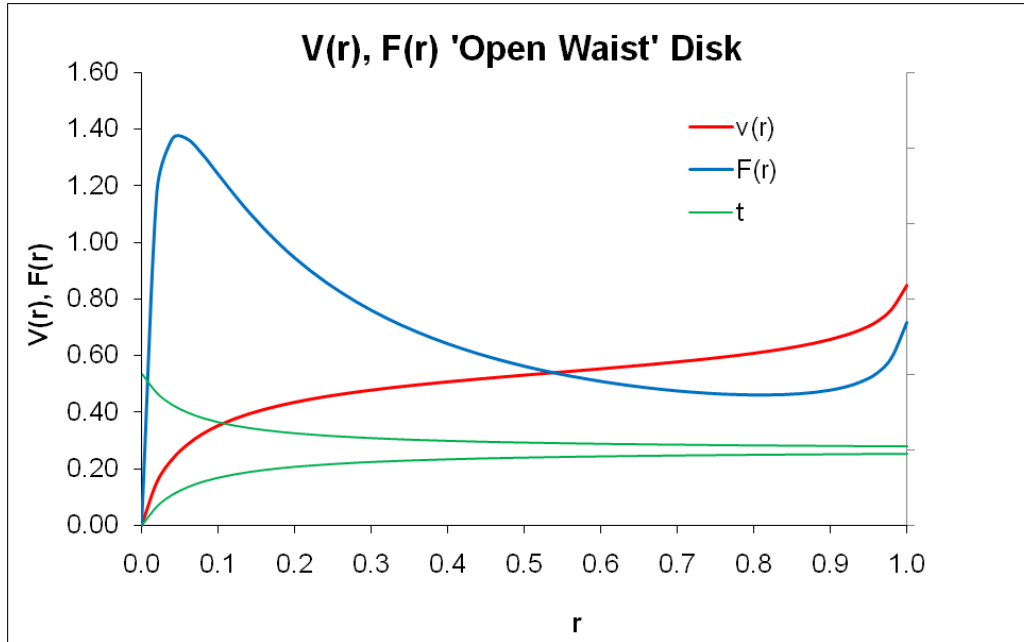


Figure 7. 'Closed waist' disk

### 2.4.4. Rotational curve Type 3

Figure 8 shows a profile with a non-zero surface density termination,  $\Sigma_0 = 1$ ,  $\Sigma_1 = 0.1$  and  $\Sigma_2 = 0.05$ , again with the equivalent disk surface density profile included for comparison. This seemingly small change produces a profound change in shape of the gravitational force and its velocity curve, with the terminal velocity increasing again after an inflection. This may be termed a Type 3 curve, broadly correlating with the 'classical' flat rotation curves that Verheijen<sup>19</sup> referred to as 'F-curves'. The disk mass is now  $M_d \approx 0.09\pi$ .



**Figure 8. 'Open waist' disk**

The significant difference between the curves of Figure 7 and Figure 8 are both a strength and weakness in this model; clearly, a range of velocity profiles can be generated, corresponding to the range of parameters selected for the profile, but by the same token, constraints on the shape of the velocity curve are weak, and are critically dependent on the surface density /disk thickness profile.

## 2.5. Gravitational force of a thin uniform disk with a central hole

Again we may assume a thin massive disk of unit uniform density/unit area, and unit radius, but with a central circular 'hole' of nominal radius  $r_b = 0.1$ . Such a disk has the form of a 'penny washer', and the gravitational potential within it falls from zero to a negative minimum (Figure 9), in a manner similar to that seen in the annulus. The gravitational potential then rises to become positive at  $r_I \approx 0.22$  before rising again within the disk to become asymptotic with that seen for the corresponding intact uniform disk of Figure 3. Because the integration is performed numerically,  $r_I$  and the magnitude of the maximum negative force,  $F_b \approx -11$ , are deduced empirically rather than analytically. Such a disk is clearly gravitationally unstable, and would require a central 'bulge' mass  $M_b \geq F_b r_I$  i.e.  $M_b \geq 0.035\pi$  for stability. The disk mass is simply  $0.99\pi$ , therefore the ratio of *disk mass:bulge mass* is  $\approx 0.99:0.035 \approx 2228:1$  for minimum stability.

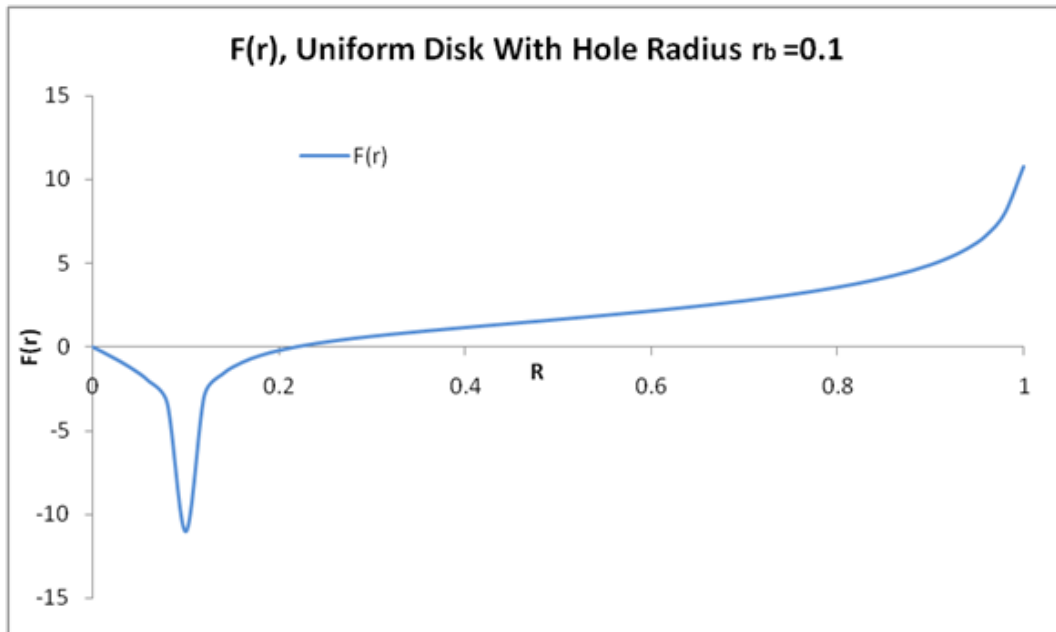


**Figure 9. Uniform 'penny washer' disk, hole diameter  $r_b=0.1$**

To obtain stability, we may insert a 'bulge' of radius  $r_I$ , and uniform density such that its total mass is some fraction of  $\pi$ . The gravitational force exerted by such a bulge is then a linearly increasing function of  $r$  out to the bulge radius,  $r_b = r_I$ ; beyond  $r_b$ , the gravitational force from the bulge is a standard inverse  $r^2$  function. By combining the two fields, we obtain the total force  $F_{tot}$  on a test particle, and can easily compute the rotational velocity for stable orbits in the resultant field,  $V_{final}$ . These curves are shown in Figure 10. The small dip in  $F_{tot}$ , and consequently in  $V_{final}$ , is a consequence of the value selected for the bulge mass.

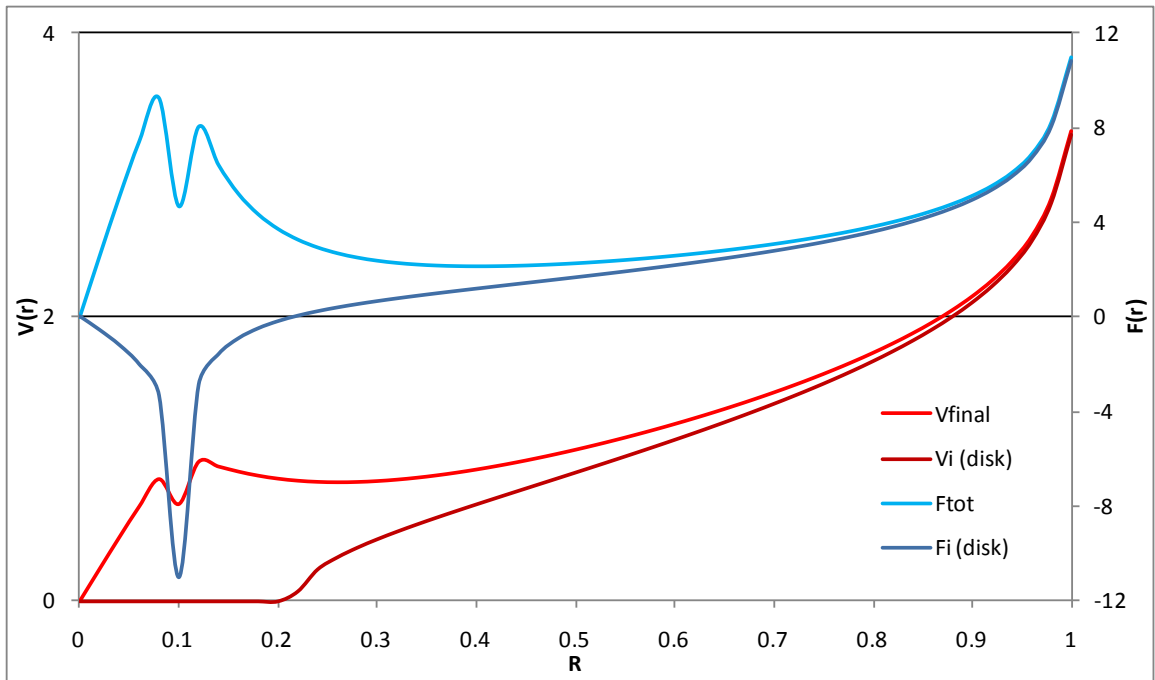


Figure 10. Resultant rotational velocity in 'penny washer' disk with bulge mass

## 2.6. The exponential disk

The previous section looked at disks with profiles such as the uniform disk, the wedge, and disks with a defined edge at  $R=1$  where the density abruptly fell to zero. This section considers some density profiles that might be considered more “natural”, such as functions of the exponential, the Gaussian curve, and a series of inverse- $r$  power curves.

The exponential disk profile has a profound place in astronomy. Surface photometry indicates that most spiral and S0 galaxies have a spheroidal bulge component whose properties differ widely between galaxies, and an exponential disk component with radial surface-brightness distribution  $I(r) = I_0 e^{-r/r_0}$  which implies a surface density distribution  $\Sigma(r) = \Sigma_0 e^{-r/r_0}$ <sup>15</sup>. The parameter  $r_0$  is the scale length of the galaxy, with dimensions of typically a few kpc (e.g. for the Milky Way,  $r_0 \approx 4\text{kpc}$ )<sup>23</sup>. Even in the presence of a prominent spheroidal component, the exponential disk contributes the major part of the total light and angular momentum. In M31 for example, >75% of the blue light and >95% of the total angular momentum come from its exponential disk<sup>24,25</sup>.

Consider a disk whose surface density profile is given by:

$$\Sigma(r) = \Sigma_0 e^{-r/r_0} \quad (2.6.1)$$

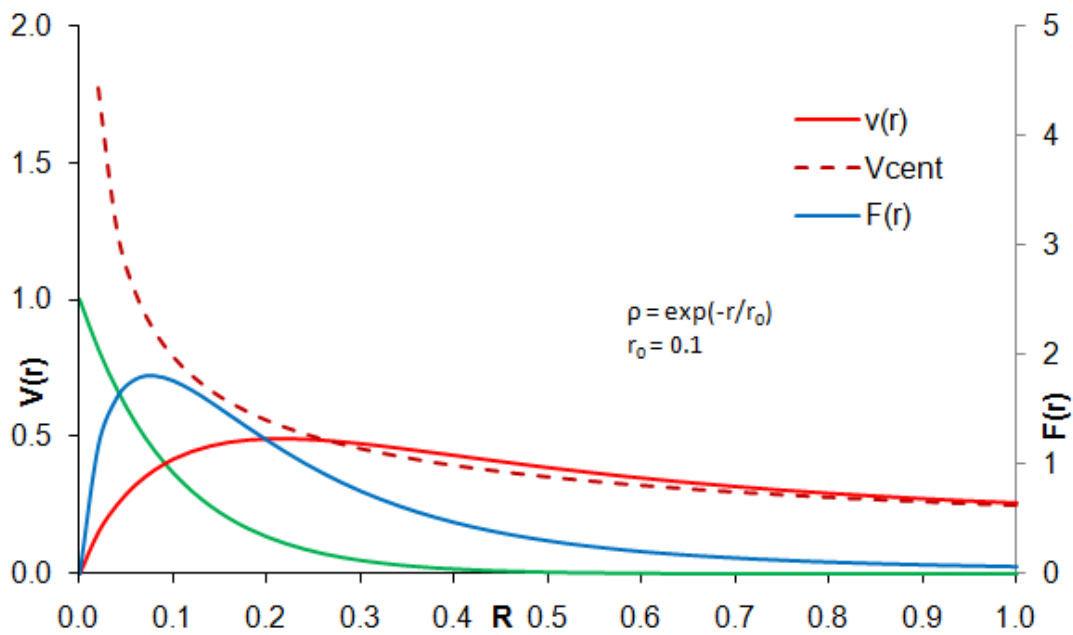


**Figure 11. Exponential disk rotation curve,  $r_0 = 0.1$**

Letting  $\Sigma_0=1$ , we may as before calculate the force  $F(r)$  on a test mass, and the resultant rotational velocity for stability,  $V(r)$ , for various values of  $r_0$ . One such curve is plotted in Figure 11 for  $r_0=0.1$ , along with the resultant disk surface density profile. The disk mass may be computed from the integral of the density profile, and is given by:

$$M_d = 2\pi r_0 \left[ r_0 - \frac{1 + r_0}{\exp(r/r_0)} \right] \quad (2.6.2)$$

e.g.  $M_d \approx 0.18\pi$  for  $r_0 = 0.1, r = 1$ .

For comparison, the rotational curve for an equivalent central mass is also shown. As expected, the two curves asymptotically converge for large  $r$ , but as  $r$  decreases the exponential curve passes through a maximum at  $r = 0.22$  before decreasing to zero, which is a Type 2 curve.

This convergence with the Newtonian curve at large  $r$  has given rise to an assumption that all galactic disks exhibiting exponential decay in their surface brightness must be integrated out to infinity to calculate their mass, and the associated velocity profile. However, the overall shape of the curve is highly dependent on the parameter  $r_0$ , which in turn is mathematically related to the radius out to which we take the cutoff point. For example, reducing the curve of Figure 11 (with  $r_0 = 0.1$ ) to a scaled radius  $r = 1/3$  is mathematically equivalent to the curve of Figure 12 with  $r_0 = 0.3$  and a sharp cut off at  $r = 1$ . This is hard to compute analytically, but is straightforward by numerical integration, and it is interesting that this curve looks superficially like a classical rotational curve, with a flattening profile for  $V(r)$ .

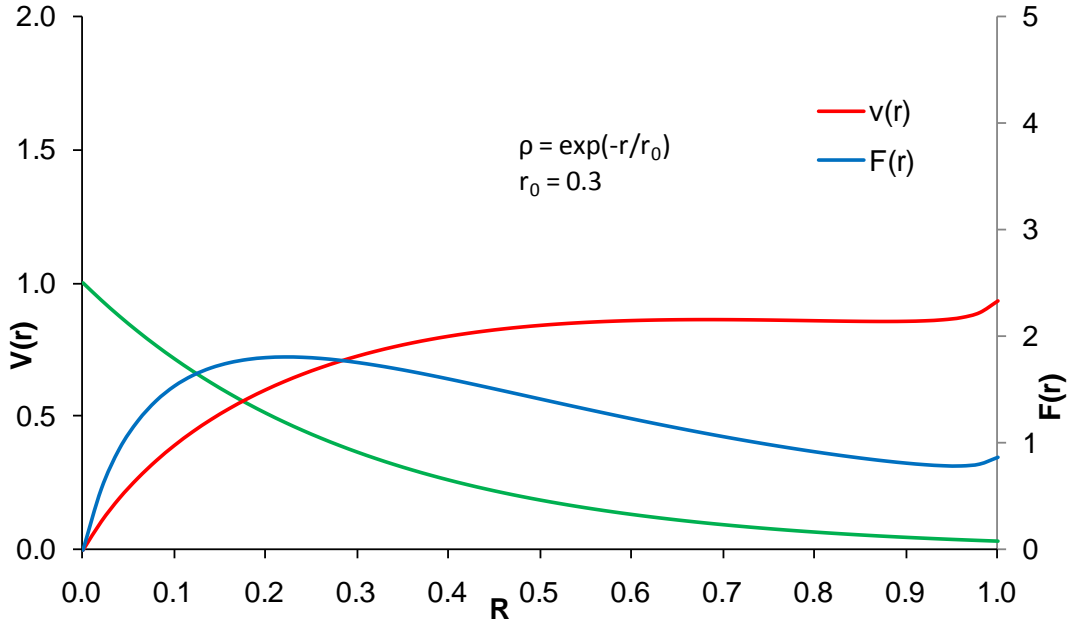


**Figure 12. Exponential disk rotation curve,  $r_0 = 0.3$**

Because of the exponential decrease in surface density with radius, reducing the curve to  $r = 1/3$  only decreases the total disk mass to  $M_d \approx 0.152\pi$ ; and, because this plot also has an abrupt edge at  $r = 1$  where the density falls to zero,  $F(r)$  and hence  $V(r)$  both show an inflection towards the disk boundary, and this is therefore a Type 3 curve. Note that this inflection is not seen in Figure 11 where the boundary surface density is only 0.00127 of its value at  $r = 1$  in Figure 12.

This transition from Type 2 to Type 3 for an exponential disk is due to changes in the cut off thickness which, as a consequence of the exponential decrease in surface density of the disk, changes rapidly with cut-off radius from a tapered to an abrupt termination. There is now considerable evidence (Section 2.16.2) that such an abrupt disk margin is a physically reality, and accounts for realistic truncated Type 3 exponential curves typified by Figure 12. Section 2.14 examines the rotational velocity profiles for a number of Low Surface Brightness (LSB) galaxies, and demonstrates how well such truncated curves can be fitted to these.

## 2.7. The rotational curve for a disk with a Gaussian profile

In a like manner, the rotational velocity curve can be computed for a disk whose theoretical surface density profile is Gaussian, e.g.:

$$\Sigma(r) = \Sigma_0 \exp\left[-\left(\frac{r}{r_0}\right)^2\right] \quad (2.7.1)$$

The disk mass is here given by:

$$M_d = \pi r_0^2 \left( 1 - \frac{1}{\exp(r^2/r_0^2)} \right) \approx \pi r_0^2 \text{ for } r_0^2 \ll 1 \quad (2.7.2)$$

with a value of  $M_d \approx 0.289\pi$  for  $r_0^2=0.3$ ,  $r = 1$ .

Similarly to the exponential curve, extending the Gaussian curve to  $r = 3$  may be considered equivalent to dividing  $r_0^2$  by a factor of 9 (Figure 13). Again, the total disk mass  $M_d$  increases only marginally, and Figure 14 also includes the curve for a central point mass ( $M_{central} = 0.0333\pi$ ) for comparison.

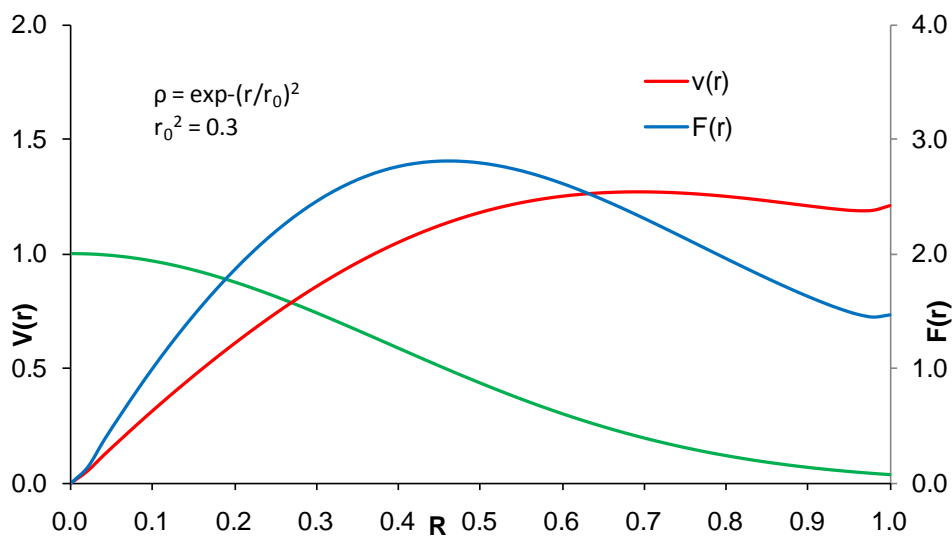


Figure 13. Gaussian curve,  $r_0^2 = 0.3$

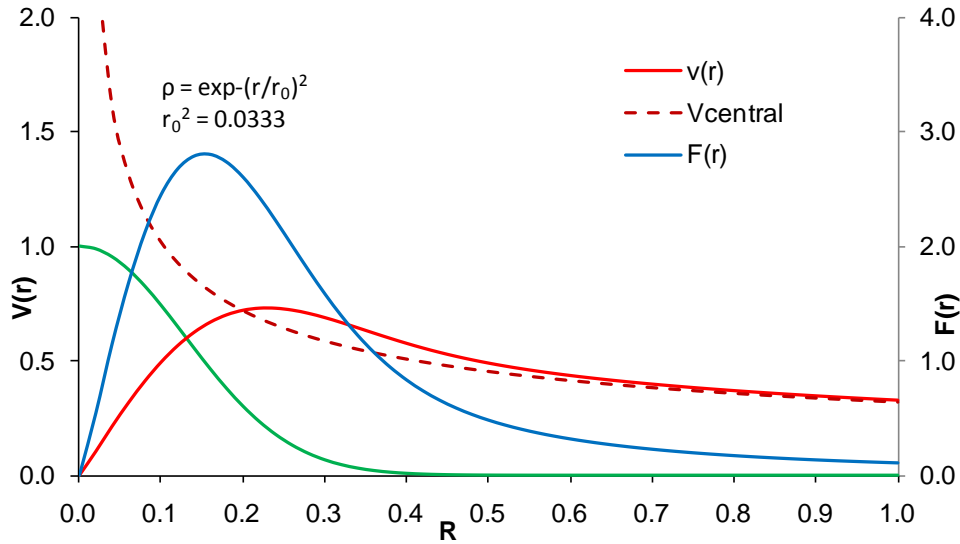


Figure 14. Gaussian curve,  $r_0^2 = 0.0333$

## 2.8. Disks with density profiles as power curves

The computational method of disk modelling can be used to fit any given surface density profile to the general disk equation to generate the resultant gravitational force and its corresponding velocity curve. In this section, we explore disk profiles described by a family of power functions of the type:

$$\Sigma(r) = \Sigma_0 r^{-a_0} \quad (2.8.1)$$

The resultant series of curves of Figure 15 are for  $\Sigma_0 = 1$  and  $a_0 = 0.5, 0.75, 1,$  and  $1.25$ . Again, the series are all plotted with an abrupt termination to the disk at  $r = 1$ , which results in the increases in rotational velocity at the end of each curve.

What is striking here is the flatness of the curve for  $\Sigma_0 \propto 1/r$ , and this is looked at in more detail in the following section.

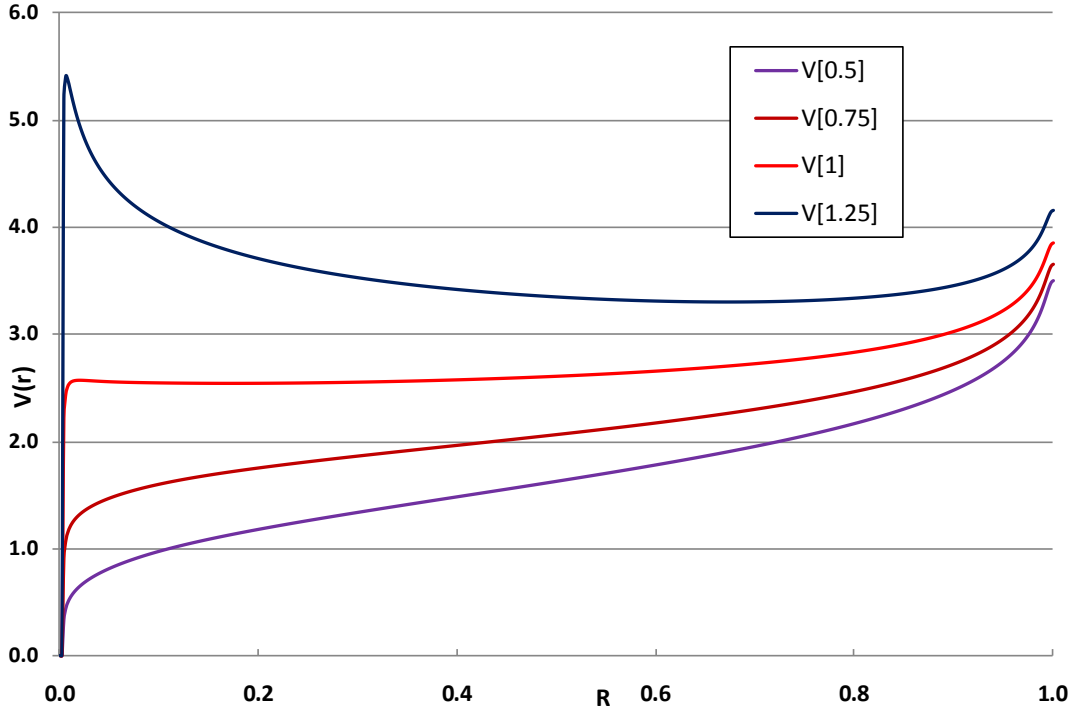


**Figure 15. Rotational curves for power series of density profiles**

### 2.8.1. Curves with disk surface density inversely proportional to $r$

For the inverse- $r$  curve of Figure 15, the total mass is simply given by:

$$M_d = \int_0^R 2\pi\Sigma_0 dr = 2\pi\Sigma_0 R \quad (2.8.2)$$

It will be noted that the mass increases continually and linearly with radius. This is an interesting result, because the infinity comes from extending the disk rather than moving to the centre, as one might have anticipated from the  $1/r$  function for density. Because of this, the shape of the curve is independent of the final radius: extending the curve beyond  $r = I$  does not alter its shape, merely the total mass, and hence – unlike the exponential curves – one cannot readily superimpose a curve for an equivalent central mass.

In general, the characteristic curves of the disks arise because, unlike spherical systems, the disk potential depends on the mass external to  $r$ . However, for a theoretical disk with  $r$  extending to infinity,  $\Sigma(r) = \Sigma_0 R_0/r$  (Mestel's disk)<sup>26</sup>,  $V_c$  is a constant with  $V_c^2(r) = 2\pi G\Sigma_0 R_0$ . This is unusual in that  $V_c(r)$  doesn't depend on the mass outside of  $r$ . However, for a galaxy with a finite cutoff at  $R_{max}$ , the disk profile will always have an abrupt cut off, and hence a rising curve at the extreme edge of the disk, unless the density is contrived to reduce gradually towards zero beyond the nominal disk radius  $R_{max}$ . These characteristics of inverse- $r$  surface density curves may be summed up as:

- The mass of the disk increases linearly with radius
- The shape of the rotation curve is scale independent
- For any finite disk, the termination will always be abrupt at some radius,  $R_{max}$
- The curve is essentially flat to within  $\pm 5\%$  out to  $r=0.77R_{max}$
- The curve rises towards its termination

### 2.8.2. Power curves with a central bulge

In a similar manner to the penny washer disks with a central bulge mass of Section 2.5, we may construct an inverse-r power curve with a central hole of radius  $r_b$ , containing a central bulge mass of the same radius with a density  $\rho_b$ .

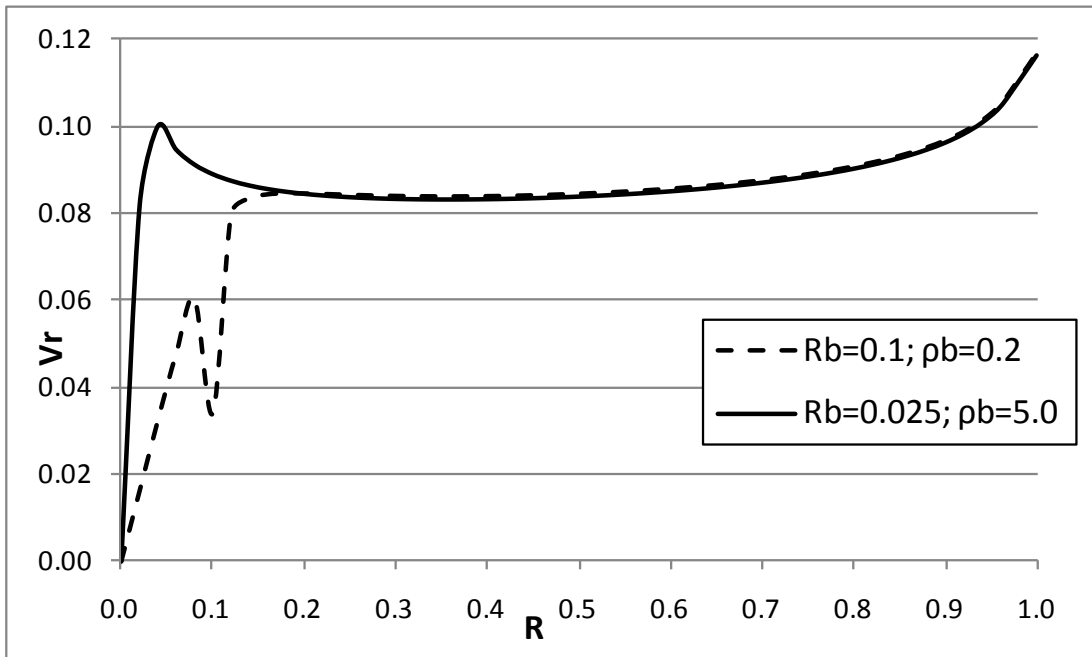


Figure 16. Disk with small, dense bulge and larger, less-dense bulge

Two such velocity curves are shown in Figure 16. These curves are identical for large  $r$ , but differ appreciably for low values of  $r$ . For a large bulge of low density ( $r_b = 0.1$ ,  $\rho_b = 0.2$ , and taking  $\Sigma_{0/disk} = 1$ ), the curve initially rises approximately linearly, but shows a dip at the bulge-disk interface. In contrast, for a small bulge of high density ( $r_b = 0.025$ ,  $\rho_b = 5.0$ ), the curve rises steeply to an initial peak, then falls away shallowly to the ‘flat’ portion before rising again at termination. Both types of curve are gravitationally stable.

### 2.9. 3-Dimensional disk rotation curves

The previous section presented an analysis of disk rotational velocities using infinitely thin disks with varying surface density to simulate real galactic disks. Real galaxies however have disks of finite thickness, and we may ask in what way do such disks differ from the theoretical models of the previous section. There is considerable controversy over the best functional form for the vertical dependence, with good fits claimed for the exponential law  $\rho_2(z) \propto \exp(-|z|/z_0)$ ; the Gaussian law  $\rho_2(z) \propto \exp(-z^2/z_0^2)$ ; the hyperbolic secant law  $\rho_2(z) \propto \text{sech}(z/z_0)$ ; and its squared version  $\rho_2(z) \propto \text{sech}^2(z/z_0)$ <sup>17</sup>.

We begin an analysis of 3-dimensional disks by considering the motion of a test particle in a uniform disk as per Section 2.3, but the disk now having finite total thickness  $2h_0$ , and uniform density  $\rho_0$ , equivalent to  $\rho_2(z) = \text{constant}$  in the standard notation. Again, the analytical calculus does not permit a simple solution, and we must rely on numerical methods. We may consider the disk to consist of a number of stacked thin disks, each of thickness  $\delta h$ , extending from  $-h_0$  to  $+h_0$ . The stable rotational velocity within each disk is shown in Figure 17 for three representative disks with  $h=0$ ,  $h=0.10$ , and  $h=0.20$ . For the disk slices near the edge, the resultant force towards the centre plane of the disk is no longer zero, and this will produce a velocity component causing the stars to oscillate across the central plane, but this motion is ignored in this simple analysis.

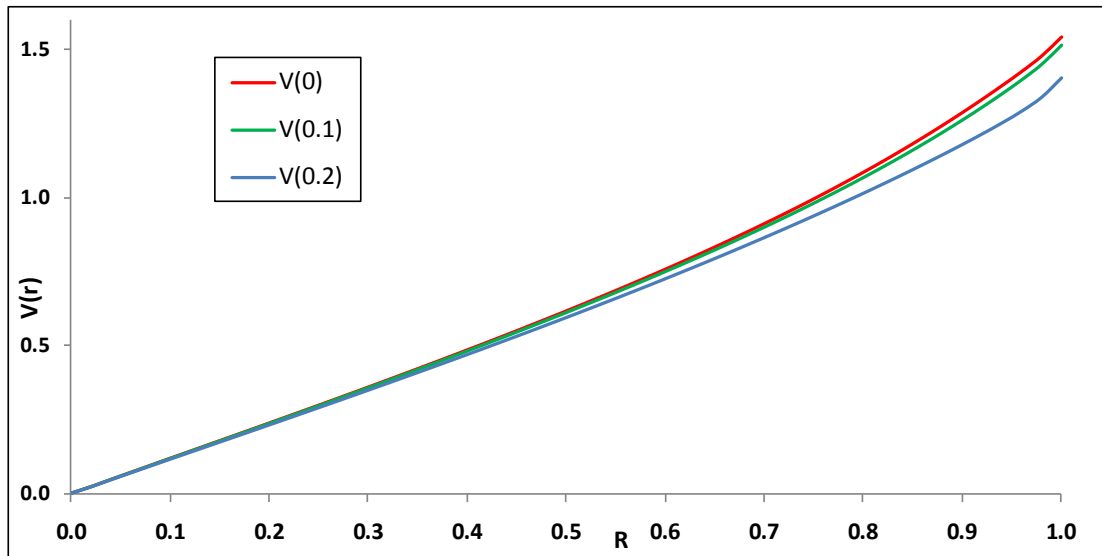


**Figure 17. 3-D model of disk rotational curves across the width of a uniform disk**

As might be expected, compared to the simple thin disk of Section 2.3, the resultant curves are flatter, because the edge effect is smeared out, but they are all strikingly similar. The implication for this in a real galaxy disk is that the rotational velocity would not be expected to vary greatly across the width of the disk.

Similar curves may be constructed for a laminar disk whose density is inversely proportional to  $r$  (Figure 18). Again, the curves remain very similar moving across the width of the disk, but there is a degree of smearing at the extremity ( $r=1$ ), the curves are less flat than for the thin disk, and rather than an abrupt change, they are more gradual in their decline towards zero at the centre.

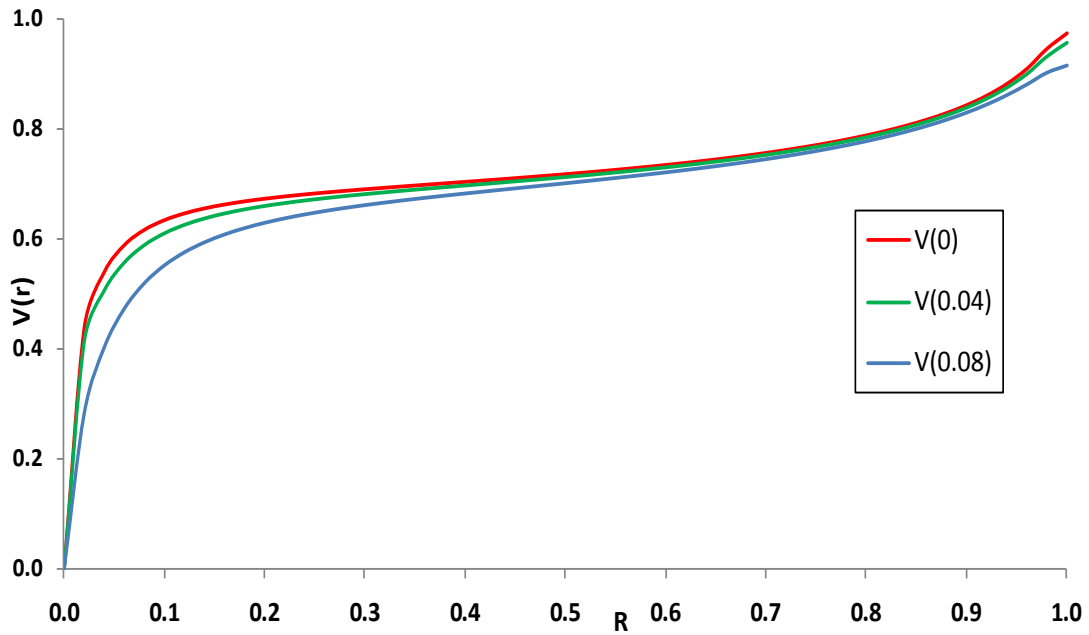


Figure 18. Thick-disk rotational curves across disk with  $\rho \propto 1/r$

## 2.10. Application of the models to real galaxies

The rotational velocity curves generated with inverse- $r$  or exponential surface density models look superficially similar to many published observations of rotational curves. What is interesting is to fit the models to the published data as accurately as possible, and see what values of bulge and disk mass are predicted by the models to obtain a good fit.

## 2.11. NGC 2915

This dark blue compact dwarf galaxy (BCD) has been well described by Meurer<sup>27</sup>, and more recently by Elson<sup>28</sup>. NGC 2915 is shown to have HI well beyond its detected optical extent, and its rotation curve is well determined. Meurer fits his curves using an extensive dark matter halo, but as may be seen below (Figure 19), the inverse- $r$  model also fits the curve well over its whole range. The parameters used to generate this curve are shown in Table 1, with the relevant parameters from Meurer's paper included for comparison.

Table 1. NGC 2915 parameters for inverse- $r$  model

Parameter	Model Value	Meurer Value <sup>27</sup>
R-bulge	2.4 kpc	1.2 – 2.8 kpc
R-disk	16 kpc	14.9 kpc
$\rho$ -bulge	0.0796 $M_{\odot}/\text{pc}^3$	0.058 – 0.1 $M_{\odot}/\text{pc}^3$ (DM Halo)
$\Sigma_0$ -disk (surface density)	0.196 $M_{\odot}/\text{pc}^2$	
Mbulge	4.61x10 <sup>9</sup> $M_{\odot}$	
Mdisk	1.67x10 <sup>10</sup> $M_{\odot}$	9.58x10 <sup>8</sup> $M_{\odot}$ (disk HI mass)

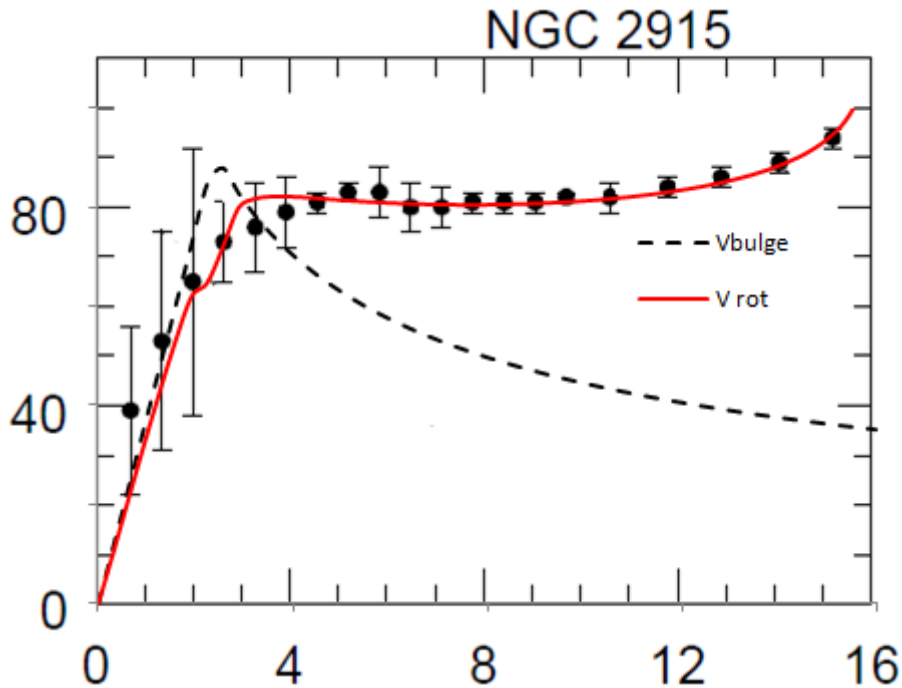


**Figure 19. NGC 2915 observed data<sup>2,27</sup> vs. model rotation curve**

Several points may be noted. The model densities for the bulge and disk are comparable to the DM halo densities in the models presented by Meurer. The total mass of the inverse-r model is  $2.13 \times 10^{10} M_{\odot}$ , a factor of x20 greater than the HI mass of Meurer. However, the model only predicts the total mass of the bulge+disk galaxy; it has nothing to say about the composition of the mass, which may equally be HI/stars +DM. The model only claims that the majority of the mass is constrained to the disk, and that this is sufficient to generate the observed rotation curve.

It may also be noted that the model predicts a terminal rise in the RC. As previously discussed (Section 2.8.1), this is an axiomatic feature of the inverse-r model, and will always be seen in association with an abrupt termination to the disk mass.

## 2.12. M31

M31 is one of the best studied galaxies, and consequently Figure 20 includes corrections for the core mass (assumed to be  $1.4 \times 10^8 M_{\odot}$ ) and the observed HI component. Data are adapted from Carignan et al<sup>29</sup> with additional data from Rubin<sup>30</sup>. The derived velocity curve accurately models the data out to 35 kpc; beyond that, with a radial cutoff at 40kpc, the curve shows the characteristic rise; but this would not be apparent if the radial cutoff had been extended further.

**Table 2. M31 parameters for inverse-r model**

Parameter	Model Value	Carignan Values <sup>29</sup>
R-bulge	6.9 kpc	-
R-disk	40 kpc	35 kpc
$\rho$ -bulge	$0.109 M_{\odot}/\text{pc}^3$	-
$\Sigma_0$ -disk (surface density)	$1020 M_{\odot}/\text{pc}^2$	-
Mbulge	$1.50 \times 10^{11} M_{\odot}$	$1.1 \times 10^{11} M_{\odot}$ (DM Halo mass)
Mdisk	$2.12 \times 10^{11} M_{\odot}$	$2.3 \times 10^{11} M_{\odot}$ (stellar mass) $5.0 \times 10^9 M_{\odot}$ (HI mass)

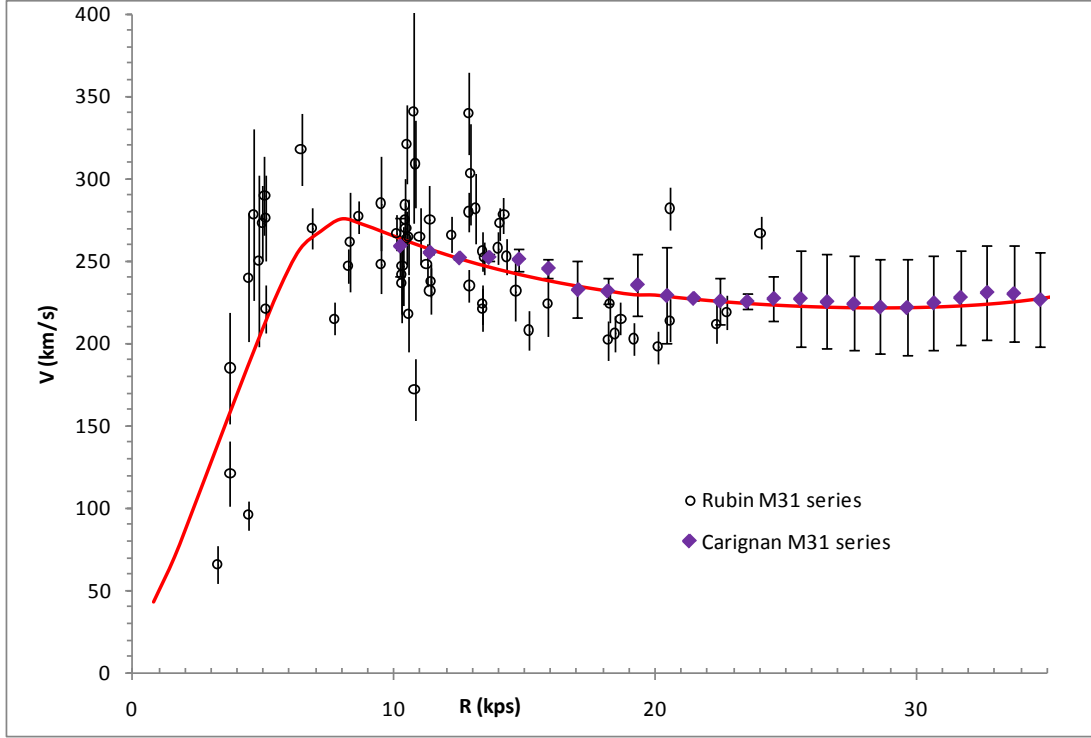


**Figure 20. M31 data<sup>29,30</sup> and model rotation curve**

### 2.13. NGC 2841

NGC 2841 is a regular early-type spiral galaxy, rather isolated, with no morphological signs of past interaction<sup>31</sup>. The observational data are derived from Sanders<sup>2</sup> and Bottema et al<sup>32</sup>. The superimposed plot of Figure 21 is for a bulge disk, with inverse-r surface density distribution, and an extended disk cutoff radius of 60kpc for an assumed distance of 15.6 Mpc. Characteristics for the model are presented in Table 3, which also compares some MOND-derived values from Bottema. This curve is presented to demonstrate the close fit that may be obtained before any correction for variations in density across the disk, or the HI gas and halo components, and despite the presence of considerable irregularities in surface density across the disk. Again, the only rule is for Newtonian gravity in a thin disk, without recourse to dark matter or MOND corrections.

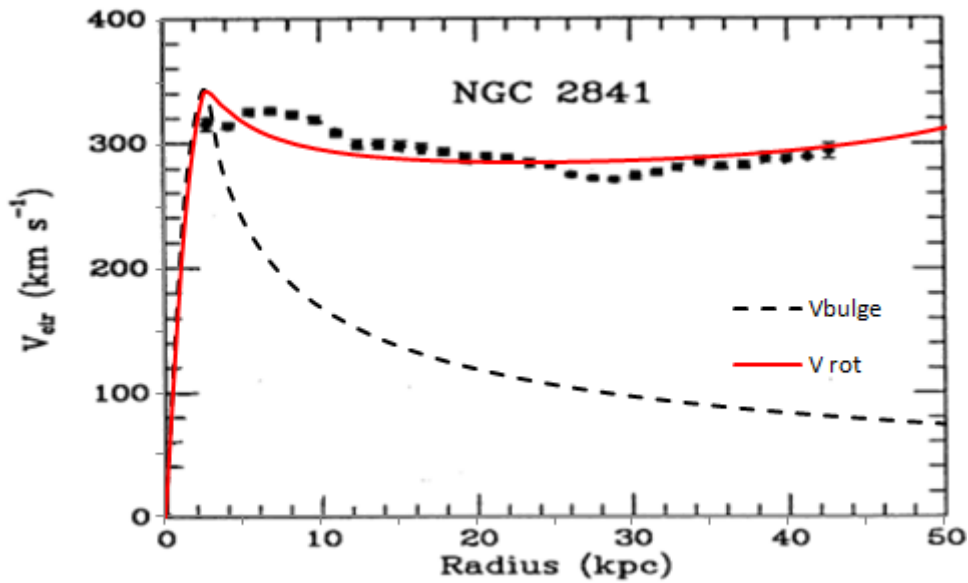


Figure 21. NGC2841 data<sup>2</sup> vs. model rotation curve

Table 3. NGC 2841 Model and Observational Parameters

Parameter	Model Value	Bottema Value <sup>32</sup>
R-bulge	1.85 kpc	-
R-disk	60 kpc	70 kpc*
$\rho$ -bulge	$1.6 M_{\odot}/\text{pc}^3$	-
$\Sigma_0$ -disk (surface density)	$2.72 M_{\odot}/\text{pc}^2$	-
M <sub>gas</sub>	-	$2.7 \times 10^{10} M_{\odot}$
M <sub>bulge</sub>	$6.63 \times 10^{10} M_{\odot}$	$1.5 \times 10^{10} M_{\odot}$
M <sub>disk</sub>	$9.95 \times 10^{11} M_{\odot}$	$2.97 \times 10^{11} M_{\odot}$ (MOND best fit)

\*Assumes a distance of 15.6 Mpc.

## 2.14. Low Surface Brightness (LSB) Galaxies

A series of 15 rotation curves for low surface brightness (LSB) galaxies were described by de Blok and McGaugh<sup>5,33</sup> who showed that MOND curves could be fitted with reasonable accuracy. Many of these rotation curves may also be fitted with curves derived from the disk models, often with equal accuracy, and a sample of these is presented here using the exponentially decreasing  $\Sigma$  models (Figure 22, Figure 23, and Figure 25).

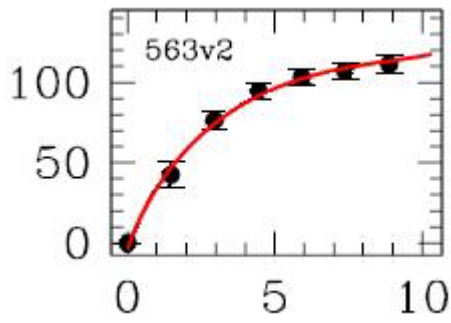


Figure 22. F563-V2<sup>5</sup>; exponential  $\Sigma$ .

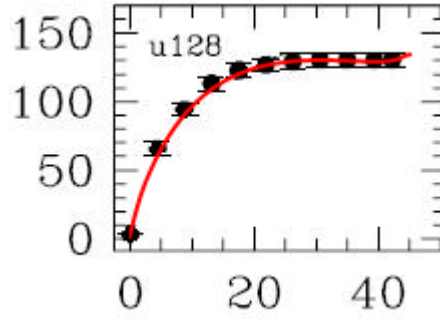


Figure 23. u128<sup>5</sup>; exponential  $\Sigma$ .

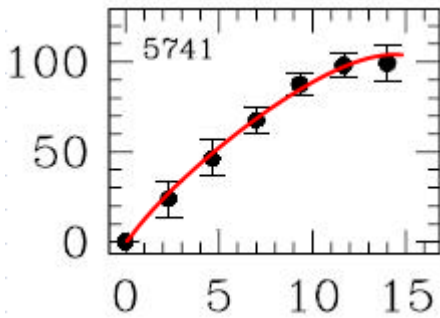


Figure 24. F574-1<sup>5</sup>; wedge  $\Sigma$ .

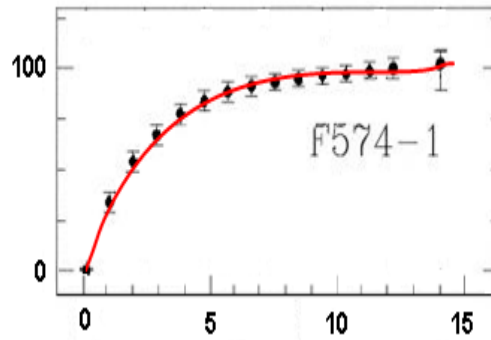


Figure 25. F574-1<sup>34</sup>; exponential  $\Sigma$ .

Note that F574-1 is a highly inclined galaxy, and the spatial smearing of HI from larger radii into the observed central depression leads to an apparent solid-body-like rotation curve when presented in the HI maps of BMH (Swaters et al<sup>34</sup>). Fitting this curve requires a central bulge, or a wedge-shaped  $\Sigma$  profile curve (Figure 24). However, Swaters et al combined their H $\alpha$  data with the HI data presented in BMH to generate the data for the curve of Figure 25<sup>34</sup> which now fits a standard exponential surface density curve with a short cutoff (Figure 12), in a similar manner to the other LSB galaxies.

**Table 4. LSB Galaxy Model Parameters**

	r0	Rb (kps)	Rmax (kps)	$\Sigma$ -disk ( $M_{\odot} \text{ kps}^{-2}$ )	Mdisk ( $M_{\odot}$ )
563v2	4.5	-	12.0	$1.60 \times 10^9$	$2.42 \times 10^{10}$
u128	13.4	-	48.0	$7.70 \times 10^8$	$1.21 \times 10^{11}$
F574-1	9.8	-	31.0	$5.80 \times 10^8$	$4.59 \times 10^{10}$

All the LSB galaxy rotational curves can be fitted with reasonable accuracy assuming only an exponentially decreasing surface density. Better accuracy could no doubt be obtained by including the gravitational fields for gas clouds and a central nucleus, but the purpose in presenting this series is to suggest that reasonably good fits can be generated using standard Newtonian gravitational forces, without recourse to dark matter halos or non-Newtonian gravity. The main requirement for fitting curves of this type is that the

exponential disk mass either extends beyond, or has an abrupt cutoff close to, the observational limit.

## 2.15. Bright Compact Galaxies – NGC 2683

Casertano and Gorkom<sup>22</sup> have described a number of HI rotation curves with a large velocity decrease in the extended region. One example using their data is shown in Figure 26 for NGC2683. Modelling this requires a large bulge of radius 1.5 – 2 kpc and mass  $\approx 2.5 \times 10^{10} M_{\odot}$ , with a disk mass of  $\approx 5.5 - 12 \times 10^{10} M_{\odot}$ , and disk radius extending for at least 50% beyond the observed radius. Two curves are shown Figure 26 for exponential and inverse-r surface density models (solid and dashed red lines respectively). It must be noted that neither fit well; however the mean of the two is an almost exact fit over the range of observed data points (blue line). The main point here is not to determine the exact surface density profile, which appears to be a blend between the two models, but to emphasise that the observed curves for bright compact galaxies, with their atypical terminal decline, can also be modelled using only Newtonian gravitational fields, without MOND or a DM halo.

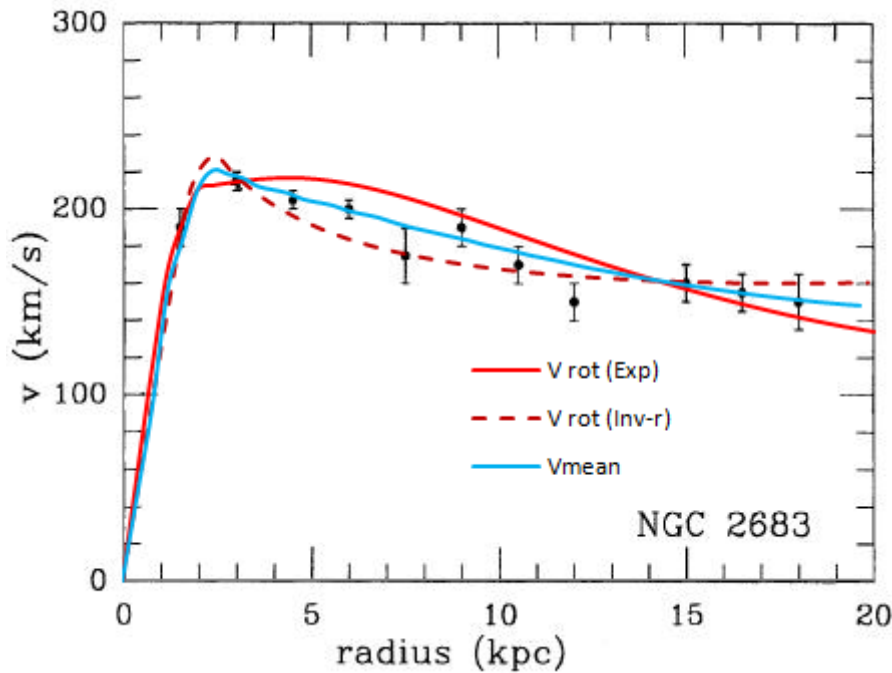


Figure 26. NGC 2683 data<sup>2</sup> vs. models with exponential  $\Sigma$  and inverse-r  $\Sigma$ <sup>22</sup>

## 2.16. Tully-Fisher relationship

In their classic paper of 1977<sup>35</sup>, Tully and Fisher (T-F) proposed that:

- 1) Intrinsic luminosity of a galaxy should correlate with total mass
- 2) Total mass is a derivative of the global profile width, and therefore linearly dependent on distance
- 3) Comparison of total mass with parameters such as hydrogen mass, luminosity and neutral hydrogen surface density could be used as a distance tool
- 4) Correlation was noted between HI profile widths and luminosities among late type spirals and irregulars
- 5) The principal correlation should be with luminosity, with modest, if any, type dependence.

This correlation is the Tully-Fisher relation, with infrared luminosity  $I_r = 220 \times V_{rot}^4$  solar luminosities if  $V_{rot}$  is given in units of km/sec. Although it was originally claimed that the maximum rotation velocity was dependent on morphological type, T-F contended that this correlation was primarily an accident of the fact that the earlier systems that were studied were intrinsically larger than later systems.

In this section, two of the earlier models, the exponential and the inverse-r, are considered for consistency with the T-F relation.

### 2.16.1. Inverse-R curves

One problem for galaxy disk models is to choose an appropriate cut off radius,  $R_{max}$ . For exponentially decreasing disks, the total mass is well defined, and the surface density will always approach zero rapidly for large  $r$ . For inverse-r models, this does not hold true; the disk mass continues to increase linearly with radius, and the total mass must be defined in terms of a cutoff radius,  $R_{max}$ .

### 2.16.2. The disk boundary in spiral galaxies

Van der Kruit and Searle<sup>36</sup> modelled the three-dimensional photometry of edge-on spirals to compute their structure. Besides demonstrating an exponential dependence of surface brightness upon  $R$  with a scale length  $h$ , their models required a very sharp cut-off at a radius  $R_{max}$  of a few scalelengths of  $h$ , with an  $e$ -folding less than about 1 kpc. This set an upper limit of about 10 km/s to the radial velocity dispersion in the stars near  $R_{max}$ .

An analysis of the profile of disk boundaries has been presented by Bizyaev and Zasov<sup>37</sup>. Although the azimuthally averaged brightness of the stellar disk in spiral galaxies decreases with galactocentric distance  $R$ , obeying in most cases an exponential law, analyses of the brightness profiles out to extremely faint isophotes suggest in many cases that the profile steepens abruptly at some large distance, defined as the disk cutoff radius,  $R_{max}$ . However, the number of galaxies with observed cutoffs in their stellar disks is small due to technical difficulties in carrying out photometry at low intensity levels, and galaxies showing cutoffs are usually edge-on galaxies in which the brightness is enhanced by projection effects. This cutoff of the disk brightness profile by itself does not imply a total absence of gas and stars at large galactocentric distances. In a number of cases, rotating HI disks extend far beyond the optical boundary, and isolated star-forming regions can sometimes be seen very far from the galactic centres. The distance  $R_{max}$  in

units of the disk scale length  $r_0$  varies over a wide range, and lies in the interval 3–5 in most cases, with the ratio  $R_{max}/r_0$  tending to increase toward larger galaxies<sup>37</sup>.

The HI profile width is often taken as a standard diameter for galactic measurements<sup>38</sup>. Bizyaev and Zasov<sup>37</sup> comment that the radial velocity dispersion of the stars in the disk (10–20 km/s for regions near the disk periphery) “smears out” the edges, so the cutoff cannot be completely sharp, and the uncertainty in  $R_{max}$  estimates can exceed 1–2 kpc. They suggest that gravitational instability is a crucial factor determining the efficiency of star formation (the star-formation rate per unit gas mass), at least in the outer regions of galactic disks. However, observations of relatively nearby galaxies show that stars are still born in places where the observed gas density is below the critical threshold, albeit at lower rates (e.g. in M33). Therefore, faint extensions of stellar disks may exist even at  $R > R_{max}$ <sup>37</sup>.

### 2.16.3. The disk boundary in galactic models

For a disk of uniform volume-density,  $\rho_0$ , it is useful to consider a critical disk thickness,  $h_{crit}$ , such that observations on the disk can no longer be performed. This critical thickness may represent one of several possible limits, such as the radius at which stars can no longer form, or the limit of visually observable stars, or the limit beyond which HI measurements cannot probe. The important thing is that such a limit will apply equally to all similar galaxies at otherwise similar distances and evolutionary history. For the classical T-F relationship, where rotational velocity is expressed in terms of IR luminosity,  $h_{crit}$  will be the radius beyond which IR becomes undetectable.

Then, given the shape of the disk envelope, we may write:

$$h = \left(\frac{h_0}{r}\right) \bar{h} \quad (2.16.1)$$

where  $\bar{h}$  is the unitary operator in kpc. Then  $R_{max}$  is given by:

$$R_{max} = \left(\frac{h_0}{h_{crit}}\right) \bar{h} \quad (2.16.2)$$

A typical set of curves for various values of the parameter  $h_0$  are shown in Figure 27. As discussed in Section 2.8.1, these curves are mathematically similar in shape, and it is therefore possible to define a common feature to compare their rotational velocities, such as the radial position  $R_{max}/2$ . It then follows that:

$$v^2 = G\rho_0 h_0 K_1 \quad (2.16.3)$$

and

$$M_{tot} = 2\pi\rho_0 \left(\frac{h_0^2}{h_{crit}}\right) \quad (2.16.4)$$

hence, eliminating  $h_0$ ,

$$v^4 = M_{tot} K \quad (2.16.5)$$

where  $K = I_{0.5}^2 G^2 \rho_0 h_{crit} / 4\pi$ .  $I_{0.5} = 13.486$  is the integral value at  $R_{max}/2$ , computed from (2.3.1) with  $\delta h = h_0/r$ .

Hence:

$$v_{rot} = 0.0034(\rho_0 h_{crit} M_{tot})^{0.25} \text{ km/s} \quad (2.16.6)$$

in units of  $M_\odot / \text{kpc}^3$ , kpc, and  $M_\odot$  respectively.

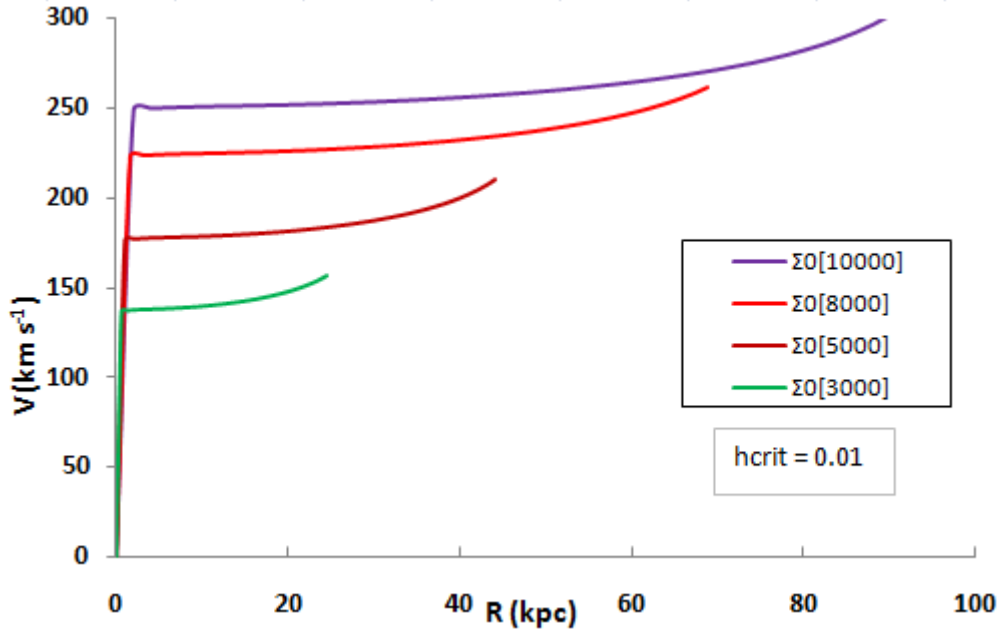


Figure 27. Inverse-r rotational curves for 4 model galaxies of differing masses

#### 2.16.4. Exponential curves

Letting the disk surface density vary as  $\Sigma_0 / \exp\left(\frac{r}{r_0}\right)$  and again assuming  $R_{max}$  to be defined by a critical cutoff,  $h_{crit}$ , we may generate a set of curves for  $V_{rot}$  for various values of  $\Sigma_0$ , as shown in Figure 28. For this set of curves,  $r_0$  was constant at 10 kpc, and  $\Sigma_0$  varied by a factor of 50:1. As discussed in Section 2.6, exponentially decreasing mass curves are not similar in shape when there is a critical limit,  $h_{crit}$ . The more massive ones have a pronounced maximum beyond which they extend considerably to approach a Newtonian limit. The low mass curves are still rising in value as the surface density reaches  $h_{crit}$ . This lack of similarity makes it difficult to define a common point for comparison of  $V_{rot}$ .

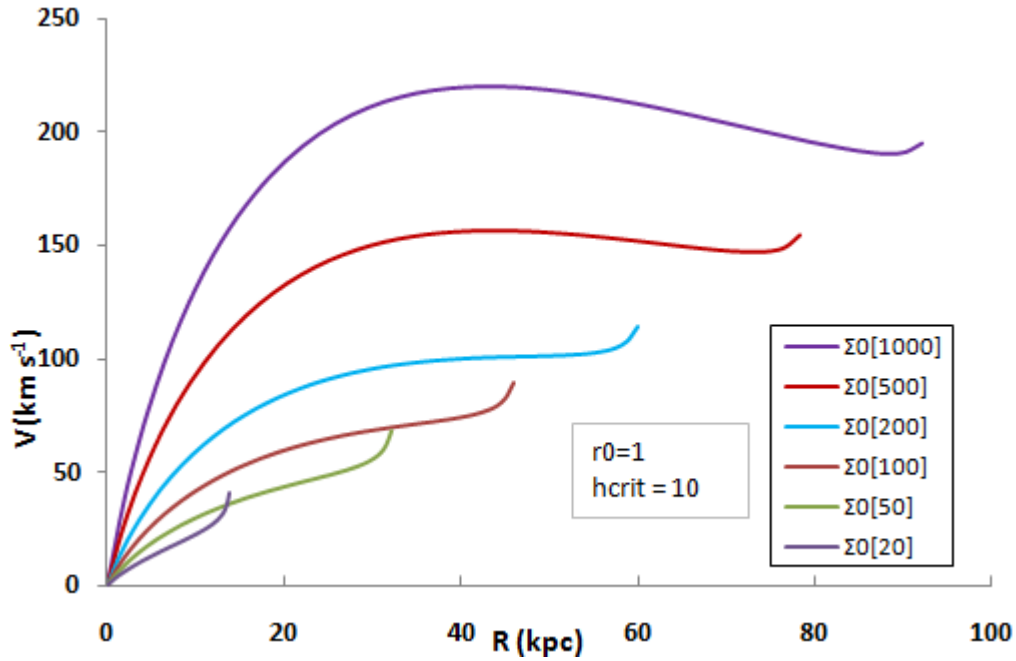


Figure 28. Exponential curves: fixed  $r_0$ , decreasing  $\Sigma_0$

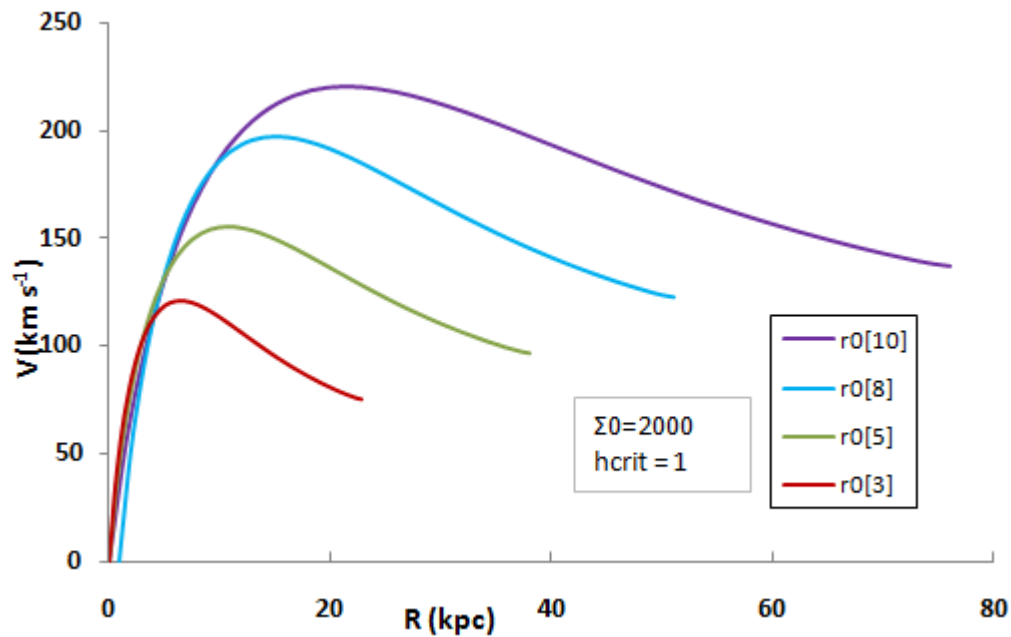


Figure 29. Exponential curves: fixed  $\Sigma_0$ , decreasing  $r_0$

A set of exponential curves is also shown for the case of fixed initial surface density  $\Sigma_0$ , but differing parameters  $r_0$  (Figure 29). These curves correspond to the observation of Freeman<sup>15</sup> that many disks have a similar value for  $I_0$  (and hence  $\Sigma_0$ ). This constancy of  $I_0$  produces the correlation between apparent magnitude and angular diameter found by Hubble. These curves are now similar, but become increasingly compressed as  $R_{max}$ , (and the corresponding  $V_{max}$ ), is reduced. Because of the similarity, it is possible to define a common position on the curves at which  $V_{rot}$  is measured, such as  $V_{max}$  or  $V_{0.5}$ , and as in Section 2.16.3, it may again be shown that  $V_{rot} \propto M_{tot}^{1/4}$ .

### 2.16.5. Tully-Fisher conclusions

Exponential disks with differing initial surface densities, but with the same exponential decay parameter  $r_0$ , present a wide variety of rotational curve profiles, and it is difficult to construct a plausible T-F relationship. However, disks with the same initial surface density,  $\Sigma_0$  but differing decay parameters, are similar in shape and do conform to the T-F relationship. Likewise, disks with an inverse-r decreasing surface density have only one parameter and are all similar; they show a generally flat rotation curve that leads to a meaningful definition for rotational velocity for comparison between disks of differing mass. For such curves, the T-F relationship emerges naturally as  $v^4 \propto M_{tot}$  (and hence  $v^4 \propto L$ ), and this may go some way towards explaining a physical meaning to the T-F relation, and quantifying its value.

### 2.17. Summary of thin disk models

- The rotational velocity of a model galactic disk may be computed by numerical analysis for any given radially-symmetrical mass distribution, assuming only a Newtonian gravitational field and stable circular orbits.
- Using numerical integration rather than analytical methods, the surface density distribution may take any possible distribution form, such as wedge shape, exponential or inverse-r.
- The disk surface density emerges as a characteristic parameter by combining the volume density and disk thickness as a thin disk.
- Bulgeless inverse-r models require only two parameters: a characteristic surface density and a defined maximum radius; exponential galaxies require a characteristic scale length as an additional parameter.
- The presence of a bulge requires two additional parameters: the bulge mass/density, and bulge radius.
- The measurement of rotational velocities requires the presence of observable baryonic mass in the form of stars, gas etc; however, because the disk mass affects the gravitational field and hence rotational velocities so strongly, it is predicted that the classical Newtonian decay curve can never be observed.
- The termination of the exponential model galactic disks may be abrupt for small  $R_{max}$ , or taper to zero for large  $R_{max}$ . The mass of inverse-r models continues to increase linearly with radius, and always terminates abruptly for any finite galaxy.
- The models generate three characteristic curves:
  - Type 1, in which the velocity curve continues to rise with no maximum, and no flat portion.
  - Type 2, which rises to a maximum before falling away.
  - Type 3, which has an inflexion to a flat plateau followed by a secondary rise on approaching an abrupt boundary.
- The observed rotational curves of many galaxies rise to a plateau where they remain remarkably flat. The rate of rise is generally steep for bulge galaxies, but relatively shallow for non-bulge galaxies.
- The generated model curves can be fitted with good agreement to many observed curves. Two distinct patterns emerge:
  - Galaxies with a minimal bulge component (e.g. many LSBs) fit a truncated exponential curve.
  - Galaxies with a massive bulge (e.g. bright spirals) generally fit an inverse-r + bulge curve.

- By assuming a finite observable cut-off thickness, the inverse-r curves, and truncated exponential curves with constant  $\Sigma_0$  conform to the T-F relationship.
- Fitting models to the observed data predicts total galactic masses and cutoff radii which appear realistic, without recourse to MOND or DM halos. The models make no prediction about the nature of the disk mass, which may include a DM component in addition to the observable baryonic mass.

### 3. THE EVOLUTION OF GALACTIC DISKS

The models of the preceding sections all calculate the spatial rotational velocity of the disk on the assumption of dynamic stability, with no attempt to analyse galactic evolution or the effect of perturbations on the rotational motion. In this section, two approaches are used to examine the stability of these models: a) a dynamically evolving model is described which is unstable over time, but also favours the development of a uniform velocity profile, with mass moving centrally and angular momentum transferring to the periphery, while beginning to generate an inverse-r type mass-distribution model; b) a thermodynamic approach suggests that uniform velocity in the disk may evolve to favour a maximal entropy system.

#### 3.1. A dynamic model for disk evolution

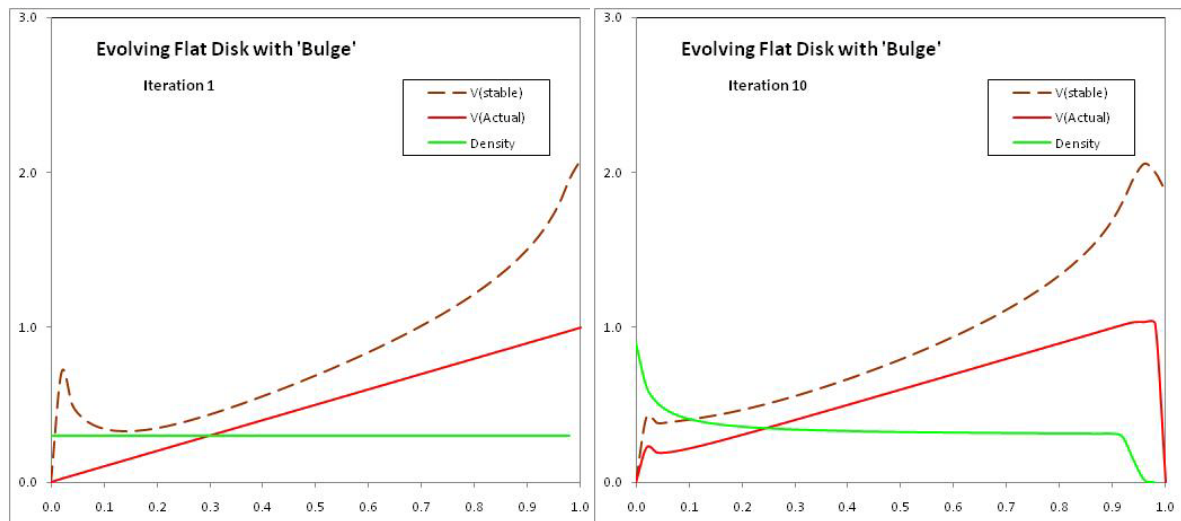
In addition to the era of separation into individual proto-galaxies, at some stage many of these galaxies must have acquired angular momentum. Although a precise mechanism for the origin of galactic angular momentum is still lacking, its presence is adequately demonstrated in the many disk type galaxies that are observed. In general terms, this may have arisen from either tidal interactions with other galaxies, or from acquired angular momentum from some phase within the early universe itself prior to separation, perhaps in a manner analogous to the early quantum fluctuations.

Griv and Gedalin<sup>39</sup> presented a detailed mathematical derivation of Jeans-Unstable density waves, and concluded that, in a thin disk, mass migrates towards the centre and angular momentum moves outwards, and – although such perturbations are difficult to analyse in detail – their conclusions have been supported by means of N-body simulations. Here, a different approach is used, developed from the previous analysis of galactic disk dynamics as the integration of all annuli in the disk.

Consider a finite disk composed of  $N$  concentric thin annuli, each with initial mass function  $m(\mathbf{r})$  and rotational velocity  $V(\mathbf{r})$  at time  $t_0$ . For each annulus, we now calculate the net gravitational force from each of the other  $N-1$  annuli through a process of integration as described in Section 2.2. This generates what may be termed the theoretical ‘stable velocity’,  $V_s(\mathbf{r})$ , for each annulus. The next step in the evolution is obtained by assuming the annulus will migrate inwards or outwards depending on whether  $V(\mathbf{r}) < V_s(\mathbf{r})$  or  $V(\mathbf{r}) > V_s(\mathbf{r})$  respectively, with movement occurring only if the velocity difference is above an arbitrary threshold. This potential for movement is calculated for each annulus, before the rings are moved, and the resultant annular masses  $m_1(\mathbf{r})$  at time  $t_1=t_0+\delta$  calculated by summation of those moving into or out of, and those remaining undisplaced, in each annulus. This ensures the conservation of mass for the ring as a whole. A new velocity is calculated for each annulus that migrates, calculated by assuming the conservation of angular momentum, so that annuli migrating inwards will speed up, and the converse. The different velocities within each annulus resulting from rings moving up or down, or staying undisplaced, are then partitioned out so that the new

annulus moves with a new uniform velocity,  $V_I(r)$  at time  $t_I$ . Finally, the new ‘stable velocity’,  $V_{sI}(r)$  at time  $t_I$  as recalculated for the new mass distribution, and the steps are repeated.

Many assumptions may be made in this type of modelling for the evolution of galactic disks, but the most drastic are what form to give the initial mass density and velocity distributions. However, some general principles may be applied. If the initial velocity is greater than the stable velocity over the radius of the galactic disk ( $V(r) > V_s(r)$  for all  $r$ ), this is highly unstable, as each annulus will migrate towards the periphery with a consequent reduction in the local stable velocity, resulting in a net dispersion of the disk. For stability, we therefore select  $V(r) < V_s(r)$  over the whole disk. A typical run is presented below in Figure 30. Here, the mass was assumed drawn out in a uniform manner (solid green line), while the velocity of the resulting disk increased linearly towards the periphery (solid red line). The dashed line shows the resultant calculated theoretical ‘stable velocity’  $V_s(r)$  across the disk. It may be seen with this type of model that, with  $V(r) < V_s(r)$  throughout the disk, there is a net migration of mass towards the centre, resulting in a gradual thinning of the disk, but with a cutoff boundary where the mass falls to zero. The mass distribution begins to approximate an inverse- $r$  pattern, and the resultant velocity begins to flatten off towards a uniform velocity distribution across the disk. A small central ‘bulge’ mass was also assumed in this model for stability. It may be seen that, beyond the disk boundary, the theoretical velocity falls off in the classical Newtonian pattern, but of course this will not be observed because there is now no mass in this region. It is worth emphasising that, in this model, galactic mass and angular momentum are conserved throughout, whatever initial conditions are ascribed.



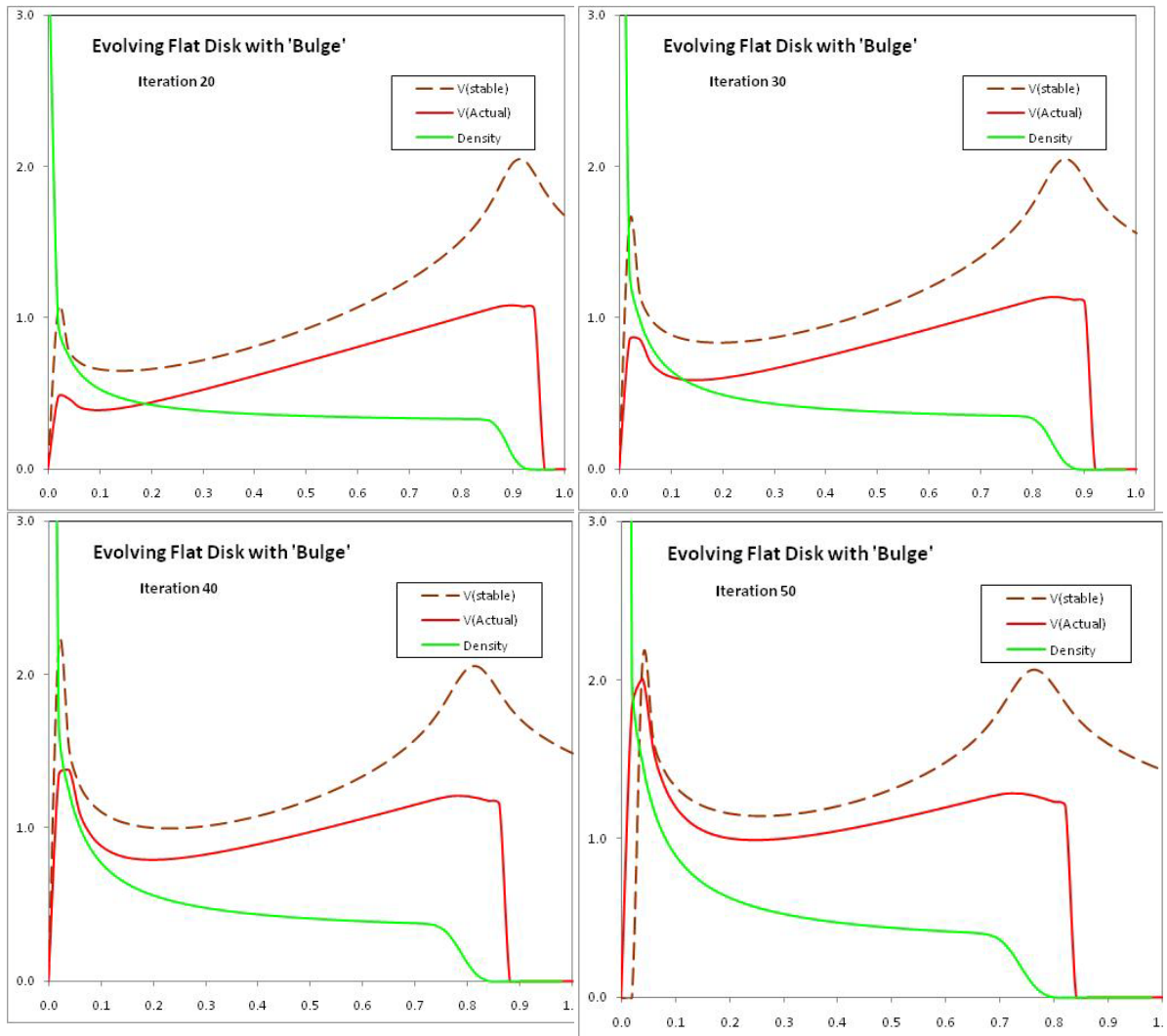


**Figure 30. Evolution of a stable disk galaxy (see text)**

Two interesting variations become evident with this type of dynamic evolutionary modelling. If the actual velocity crosses the stable velocity from a higher value with increasing  $r$ , at a distance  $R_c$ , then annuli from  $r < R_c$  move out, but meet annuli from  $r > R_c$  moving inwards, and the disk mass begins to increase locally as a reinforcing instability develops with mass enhancement. The opposite situation occurs when  $V(r)$  crosses  $V_s(r)$  from lower to higher; then rarefaction occurs as mass moves away from the node. This later situation is illustrated in Figure 31, where the instability is sufficiently severe that the disk is split, with the outer segment being flung into space away from the developing disk, with consequent loss of disk mass and angular momentum to the system. It is worth noting, however, that the disk segment remaining is stable, and again begins to take on the flat velocity curve associated with observed galactic disks.

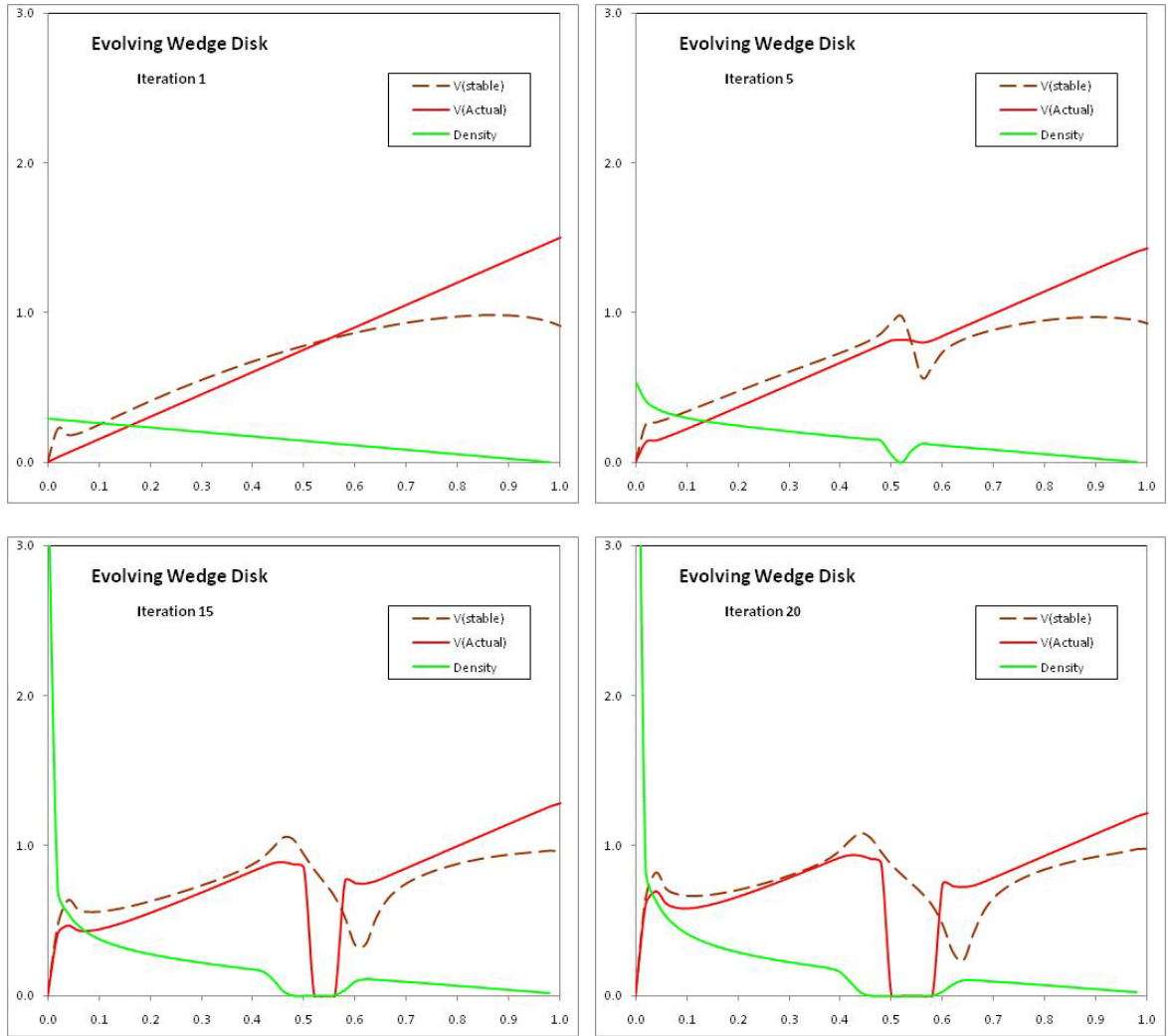


**Figure 31. Evolution of density instability**

The models illustrated in this paper have been selected to present the simplest patterns of disk evolution, but patterns of alternating density enhancement and rarefaction also arise quite frequently in some plausible models, and these suggest a mechanism for such variations to arise in real disks, which would then wind up through differential velocity flows to develop the familiar galactic disk spirals.

### 3.2. A thermodynamic analysis of the galactic disk

An isolated galaxy may be considered, for much of its existence, to be an independent collisionless assemblage of discrete particles (stars), interacting with each other gravitationally. An important consequence is that several independent physical parameters of the system are conserved, such as the overall number of particles, and hence the total mass, the total angular momentum, and the total internal energy as a summation of kinetic energy and gravitational potential energy. Thermodynamically, this is defined as a micro canonical ensemble, and such a system can only undergo adiabatic changes, being isolated from any external transfer of energy, so the initial parameters are fixed and invariant. To a reasonable approximation, a disk galaxy may also be considered time invariant, i.e. stable, with a stable mass distribution in stable orbits, equivalent to a thermodynamic system in thermal equilibrium.

Although the interactions between particles in the galactic disk are gravitational and attractive, in contrast to the electrostatic repulsive forces of molecules in an ideal gas, nevertheless the interactions are elastic so the mean kinetic energy throughout the disk is equalised, which is equivalent to attaining thermal equilibrium in a thermodynamic system. Such a system, moreover, will have its entropy maximised through mixing of components. Because the volume, number of discrete particles, and internal energy are fixed (the microcanonical ensemble), such a system is one in which all states, of number  $\Omega$ , are equally likely, and the entropy of the system is given by:

$$S = K_S \ln \Omega$$

where  $K_S$  is analogous to  $K_B$ , the Boltzmann constant in thermodynamics. The entropy is here maximised because we have lost all information about the initial conditions except for the conserved variables.

A sufficient condition for thermal equilibrium is for the mean kinetic energy within the system to be equalised throughout the disk system. It may immediately be seen that the only distribution of matter satisfying this condition is the inverse- $r$  model, because the mass of each annulus is then approximately uniform and, as was shown in Section 2.8.1, this distribution also generates a uniform and stable velocity profile.

#### 4. MODEL FOR A SPHERICAL GALAXY

The virial theorem is a powerful tool for analysing the motion of stars in an idealised galaxy, wherein the potential energy (PE) function is generally taken to be the PE of a mass  $m$  brought from infinity (which defines the zero point for the PE function) towards a self gravitating galaxy of total mass  $M$ . By assuming from Newton's work that  $m$  is at a radial distance  $r$  from the centre, and all mass within the sphere defined by  $r$  is equivalent to a point mass at the galactic centre, and all mass external to that sphere may be ignored, the usual gravitational force  $F \propto 1/r^2$  is applied, and the standard equations of motion for the star system are derived.

However, in the early universe (defined here as the epoch of galaxy separation,  $T_g$ ), this standard analysis for PE may not be applicable. At this epoch of separation, the density of the universe was approximately uniform, with the exception of expected local fluctuations. Where the density is a little above the average, we may expect nucleation to occur as a precursor to the final massive core at galactic centres. Where the density is a little lower than the average, the continuing expansion of the universe may be thought of as causing splits in the distribution of matter, as though the protogalaxies were being torn apart from each other due to the expansion of space. Thus it does not make sense to talk of bringing a mass  $m$  from infinity, as the mean gravitational field was everywhere zero at this epoch.

This model for the distribution of matter in spherical galaxies therefore takes a modified approach, by assuming that the individual masses within each galaxy do not come from infinity, but are set in place during the expansion of the universe, until galactic separation was sufficient for them to become self gravitating. Neighbouring galaxies would then have had reducing mutual gravitational influence, and the initial PE function for each  $m$  would have continued to increase asymptotically towards its theoretical value had  $m$  been brought in from infinity, thus driving gravitational collapse.

At this time, it may be debated whether the matter of the universe was in the form of gas, or if early star formation had already occurred, but for the purpose of this model it may be assumed that the protogalaxies were populated by young, uniform stars, each of mass  $m$ . The uniform density of the universe at the epoch of galaxy separation may be defined as  $\rho_0$ , and the mean radius of each protogalaxy as  $R_0$ , containing a mass  $M_0$ . Although the individual masses had been separating from each other as a consequence of the overall expansion, at the epoch of galaxy separation the masses would have ceased moving relative to the proto-centre of their new galaxy, and the mean kinetic energy (KE) within each galaxy at this instant was therefore zero. As separation continued, the masses began to infall through mutual self gravitational collapse into the local gravitational field generated by the protogalaxy. The total mechanical energy of the system (PE+KE) was derived from the expansion energy of space, increasing asymptotically as neighbouring galaxies drew away, and would have been balanced by mutual gravitational slowing of the rate of expansion in this early phase.

This model assumes that self-gravitational infalling would continue with the newly acquired initial PE converted into kinetic energy as the masses accelerated inwards. The motion of each individual star is highly chaotic, and equipartition of KE throughout the system is assumed through gravitational interactions, such that the masses reach dynamic stability, finally moving with a mean scalar velocity,  $v_{av}$ . At this time, it is easy to show that a state of equilibrium would be reached in which they would undergo periodic motion, traversing a path across a sphere of final radius  $R_f$ .

#### 4.1. Assumptions of the model

- The galaxy starts at time  $T_g$  (the epoch of galactic separation) from a collapsing, self-gravitational sphere of radius  $R_0$ .
- The initial state of the protogalactic sphere may be in the form of gas, but as this collapses on itself, star systems spontaneously form which are approximately the age of the galaxy. The whole system may therefore be treated as though it were initially composed of  $n$  stars of mean mass  $m$ , with an initially uniform distribution of mass with initial density  $\rho_0$ .
- Radial symmetry about the centre.
- No angular momentum.
- The sphere collapses to a final equilibrium radius,  $R_f$ .
- The loss in  $PE$  in collapsing from  $R_0$  to  $R_f$  is converted entirely into  $KE$  of motion of the stars (conservation of energy).
- The mass of the sphere is  $M_0 = nm$  throughout (conservation of mass).
- Equipartition of energy such that, over sufficient time (but a time much shorter than the observed age of the galaxy), the total energy of the system is partitioned equally within each spherical shell, as a function of radius.
- The equations of motion depend solely on Newtonian gravitation in standard form.

#### 4.2. Equation of motion in a uniform spherical galaxy

We assume the star/gas density was approximately uniform at the epoch of galactic separation. The mean gravitational field is zero within an infinite uniform distribution of mass, but after the epoch of galactic separation, each island galaxy became increasingly isolated, with a defined centre. Thereafter, a typical galaxy became a self-gravitating sphere of particles, such as a star field, with initial radius  $R_0$  and initial uniform mean

mass density  $\rho_0$ , which was the density of the universe ( $U$ ) at the era of galactic separation (Figure 32).

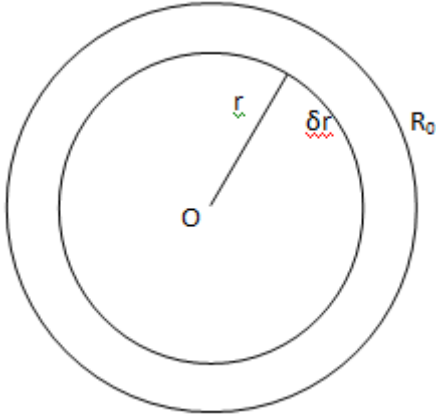


**Figure 32. Gravitational potential energy of shell of radius  $r$**

#### 4.2.1. Initial potential energy of a spherical galaxy

The gravitational force on a test mass  $m$  is:

$$F = -G \frac{mM_r}{r^2} \quad (4.2.1)$$

where  $M_r$  is the mass internal to  $r$ . The potential energy ( $PE$ ) of the mass is defined as the work done in bringing the mass from infinity to  $r$ , and is the radial path integral of  $F$ :

$$PE = G \frac{mM_r}{r} \quad (4.2.2)$$

Hence the  $PE$  of a thin shell at  $r$ , thickness  $\delta r$ , will be:

$$\delta PE = \frac{GM_r m_{shell}}{r} \quad (4.2.3)$$

The mass  $M_r$  internal to  $r$  is:  $M_r = \frac{4}{3}\pi r^3 \rho_0 \quad (4.2.4)$

the shell mass is:  $m_{shell} = 4\pi \rho_0 r^2 \delta r \quad (4.2.5)$

Hence:  $\delta PE = \frac{G \cdot \frac{4}{3}\pi r^3 \rho_0 \cdot 4\pi r^2 \rho_0 \delta r}{r} = \frac{16\pi^2 G \rho_0^2 r^4 \delta r}{3} \quad (4.2.6)$

and the total initial PE is:

$$PE_0 = \int_0^{R_0} \frac{16\pi^2 G \rho_0^2 r^4}{3} dr = \frac{16\pi^2 G \rho_0^2 R_0^5}{15} \quad (4.2.7)$$

But the total mass of the galaxy is:  $M_0 = \frac{4}{3}\pi R_0^3 \rho_0$  (4.2.8)

i. e.  $\rho_0 = \frac{3M_0}{4\pi R_0^3}$  (4.2.9)

hence:  $PE_0 = \frac{3M_0^2 G}{5R_0}$  (4.2.10)

#### 4.2.2. Final potential energy

Although starting as a sphere of uniform density, this is clearly unphysical as the sphere collapses; with uniform density, each shell would then have contained a mass of stars  $m_{shell} \propto r^2$ ; but at equilibrium the flux of stars moving into and out of a shell should exactly balance. This implies that the number density of stars in each shell should be  $\rho_{shell} \propto 1/r^2$  (as visualised in the distribution of visible stars in globular cluster M15, (Figure 33)).



**Figure 33. Globular Star Cluster M15.**  
(NASA: Hubble Heritage STScI/AURA)

Let us therefore define a density function as:

$$\rho(r) = \rho_f \cdot R_f^2 / r^2 \quad (4.2.11)$$

where  $\rho_f$  is a characteristic density at the surface of the galaxy, radius  $R_f$ . This function tends to  $\infty$  as  $r \rightarrow 0$ , and physically, this may imply the presence of a black hole at the galactic centre. The total mass is then given by:

$$M_{tot} = \int_0^{R_f} 4\pi r^2 \rho(r) dr = M_0 \quad (4.2.12)$$

i. e.  $4\pi \rho_f R_f^2 \int_0^{R_f} dr = 4\pi \rho_f R_f^3 = M_0 = \frac{4}{3}\pi \rho_0 R_0^3$  (4.2.13)

and hence:

$$\rho_f = \frac{1}{3}\rho_0 \left(\frac{R_0}{R_f}\right)^3 = \frac{M_0}{4\pi R_f^3} \quad (4.2.14)$$

where  $R_0$  and  $\rho_0$  are the initial radius and initial mean mass density respectively.

From (4.2.3) for the  $PE$  of a shell at  $r$ , thickness  $\delta r$ :

$$\delta PE = \frac{GM_r m_{shell}}{r} \quad (4.2.15)$$

where now:

$$M_r = \int_0^r 4\pi r^2 \rho(r) dr = 4\pi \rho_f R_f^2 r \quad (4.2.16)$$

and

$$m_{shell} = 4\pi \rho(r) r^2 \delta r = 4\pi \rho_f R_f^2 \delta r \quad (4.2.17)$$

Hence:

$$\delta PE = 16\pi^2 G \rho_f^2 R_f^4 \delta r \quad (4.2.18)$$

and the final total PE is:

$$PE_f = 16\pi^2 G \rho_f^2 R_f^5 = \frac{GM_0^2}{R_f} \quad (4.2.19)$$

The change of PE is therefore:

$$\Delta PE = GM_0^2 \left( \frac{3}{5R_0} - \frac{1}{R_f} \right) \quad (4.2.20)$$

### 4.2.3. Kinetic energy

The total KE for  $n$  stars of mean mass  $m$  at equilibrium is:

$$Total\ KE = \sum_1^n \frac{1}{2} m v_{av}^2 \quad (4.2.21)$$

Assuming full equipartition of energy amongst the stars in each shell, we may consider a mean velocity  $v_{av}$  at equilibrium such that:

$$KE_f = \frac{1}{2} M_0 v_{av}^2 \quad (4.2.22)$$

or, equating total KE with the decrease in PE:

$$v_{av}^2 = \frac{2KE_f}{M_0} = 2GM_0 \left( \frac{1}{R_f} - \frac{3}{5R_0} \right) \quad (4.2.23)$$

### 4.2.4. Periodic motion of stars within a sphere with increasing density

The equation of motion of a star of mass  $m$  within a gravitational sphere with a density inversely proportional to  $r^2$  is given by:

$$F = m\ddot{r} = -G \frac{mM_r}{r^2} = -Gm \frac{4\pi \rho_f R_f^2 r}{r^2} = -\frac{4\pi G \rho_f R_f^2 m}{r} \quad (4.2.24)$$

or 
$$\ddot{r} = -\frac{C_1}{r} \quad (\text{where } C_1 = 4\pi G\rho_f R_f^2) \quad (4.2.25)$$

This may be solved analytically by considering the change in PE of  $m$  as it falls across the sphere. The  $PE$  is the work done in bringing the test mass  $m$  towards the centre against the gravitational field,  $F$ . Defining the zero of  $PE$  to be at the galactic surface,  $R_f$ , and  $\Delta PE$  to be the change in  $PE$  in moving from  $R_f$  to  $r$ , then:

$$\Delta PE = -m \int_{R_f}^r -\frac{C_1}{r} dr \quad (4.2.26)$$

$$i.e. \Delta PE = mC_1 \left( \log(r) - \log(R_f) \right) = -mC_1 \log\left(\frac{R_f}{r}\right) \quad (4.2.27)$$

Using the conservation of energy,  $\Delta KE + \Delta PE = 0$ :

$$\Delta KE = mC_1 \log\left(\frac{R_f}{r}\right) = \frac{1}{2}mv^2 \quad (4.2.28)$$

Rearranging, and using  $v = dr / dt$ :

$$dt = \frac{dr}{\sqrt{2C_1 \log\left(\frac{R_f}{r}\right)}} \quad (4.2.29)$$

This has a standard integral solution<sup>40</sup>:

$$\int \frac{1}{\sqrt{\log\left(\frac{a}{x}\right)}} dx = -a\sqrt{\pi} \operatorname{erf}\left(\log^{\frac{1}{2}}\left(\frac{a}{x}\right)\right) \quad (4.2.30)$$

where  $\operatorname{erf}(z)$  is the integral of the Gaussian distribution.

$$i.e. \quad t = \left| -\frac{R_f\sqrt{\pi} \operatorname{erf}\left(\log^{\frac{1}{2}}\left(\frac{R_f}{r}\right)\right)}{\sqrt{2C_1}} \right|_{r=R_f}^{r=0} \quad (4.2.31)$$

which is a continuous and complete function, with the properties  $\operatorname{erf}(0) = 0$ , and  $\operatorname{erf}(\infty) = 1$ . The time for  $m$  to fall towards the centre (a quarter cycle) is therefore:

$$T_{1/4} = \pm \sqrt{\frac{1}{8G\rho_f}} \quad (4.2.32)$$

where  $T$  is the time for a full cycle. The emergence of the error function in this integral might be anticipated from remembering that the velocity of any particle in a system at thermal equilibrium will have a normal distribution due to the maximum entropy principle. This implies that the integral will have a log normal distribution.

Although this simplistic approach ignores relativistic effects as the mass accelerates towards the centre, in practice the motion is highly chaotic through the action of gravitational interactions, and from any non-radial component inherited from the time of galaxy formation. This therefore causes the star to swing past the centre, apart from very rare encounters within the event horizon at the Schwarzschild radius if a black hole core is present. There is therefore a low probability of any individual star experiencing relativistic encounters, so this does not significantly affect the final result.

The mean velocity is then simply  $R_f / T_{1/4}$ , and the mean square velocity is:

$$v_{av}^2 = 8G\rho_f R_f^2 = \frac{2GM_0}{\pi R_f} \quad (4.2.33)$$

But (from 4.2.23):

$$v_{av}^2 = 2GM_0 \left( \frac{1}{R_f} - \frac{3}{5R_0} \right) \quad (4.2.34)$$

i. e.

$$\frac{1}{\pi R_f} = \left( \frac{1}{R_f} - \frac{3}{5R_0} \right) \quad (4.2.35)$$

Substituting  $\varepsilon = R_f/R_0$  and solving for  $\varepsilon$ :

$$\varepsilon = \frac{5}{3} \left( 1 - \frac{1}{\pi} \right) = 1.136 \quad (4.2.36)$$

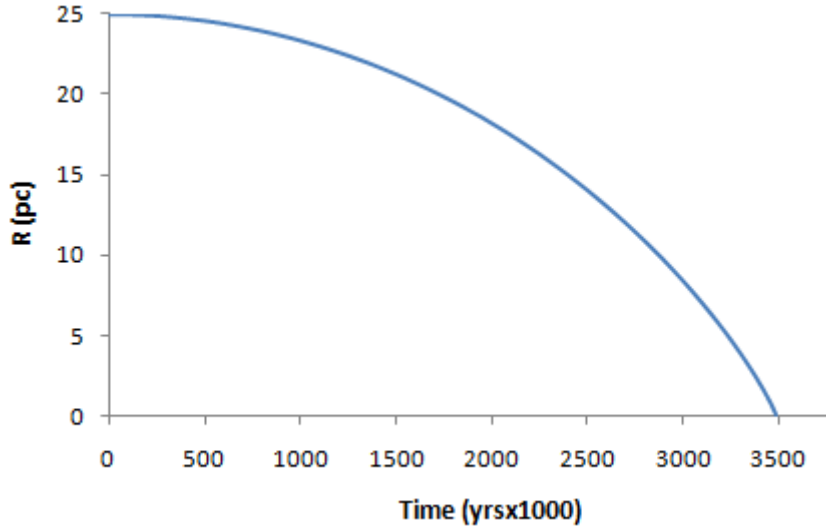
This is a remarkable result, implying that all simple spherical galaxies expand to have a stable maximum radius of approximately 1.14 times their initial radius at the epoch of galactic separation. Although physically larger, the majority of the mass is internal to the initial radius, and the total potential energy has of course decreased.

#### 4.2.5. Ratio of mean galactic separation to mean galactic radius

At the era of separation,  $T_g$ , protogalaxies had expanded to a radius  $R_0$ .  $T_g$  corresponds approximately to the epoch of decoupling, and its value will probably approximate to this epoch ( $\approx 3.77 \times 10^5$  yrs) with an upper limit at the age of the oldest galaxy thus far discovered (UDFy-38135539) of  $6 \times 10^8$  years at  $Z=8.55$ <sup>41</sup>. At that time, as galactic expansion stopped and galactic separation began, it may be asserted that – relative to the proto galactic core – the protogalaxy had a mean stellar motion of zero.

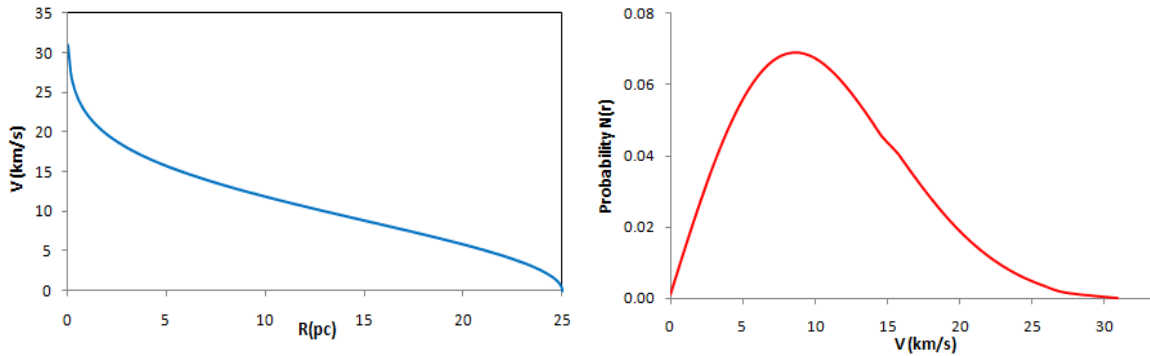
The present day separation distance between galaxies is influenced by both the continual expansion of space between them after individual galaxies separated, leading to the familiar Hubble's Law of red-shift with distance, and by mutual gravitational attraction between neighbouring galaxies, with the infalling of galactic clusters leading to galactic interactions or ultimately to complex galactic merging. Let the mean separation of galaxies at  $T_g$  be  $2R_0$ , the present mean separation between galactic centres be  $d_g$ , and taking the present age of the universe  $\approx 1.37 \times 10^{10}$  yrs<sup>42,43</sup> with an upper limit to the epoch of galaxy formation ( $T_g$ ) as  $\approx 6 \times 10^8$  yrs, then  $d_g \approx 45.7R_0$  through Hubble separation. Substituting  $R_f \approx 1.14R_0$  suggests a present ratio of mean galaxy separation distance: mean galactic diameter of  $\approx x20$ .

Figure 34 shows the mean time-distance curve for a typical star in galaxy M15, assuming a radius of 25pc and a total mass of  $4.5 \times 10^5 M_\odot$ .



**Figure 34. R-T curve for M15**

The velocity/radius curve for a typical star in M15 is shown in Figure 35, and the probability of finding a star with any given velocity increment is shown in Figure 36, normalised so that the area under the curve is 1 (i.e. certainty). Although this is a theoretical LoS probability curve across the centre of the galaxy, it is broadly in agreement with the observational velocity probability curve presented by McNamara et al<sup>44</sup>. More realistic curves to match observational values would introduce a mass distribution function for the stars; whilst more complex, the fundamental dynamics would not be changed, and as with the disk galaxies, the total mass and radius of any actual GC can be adjusted to fit the observed parameters without recourse to external DM haloes or MOND. Although the required mass may not all be detectable with current instrumentation, it might be accounted for by undetected baryonic mass, or by one form of DM obeying standard Newtonian dynamics.



**Figure 35. Predicted V-R Curve for M15    Figure 36. Velocity probability for M15**

### 4.3. The IMF and Globular Clusters.

The Initial Mass Function (IMF) for the stellar component of early galaxies has been debated for more than 50 years, since Salpeter<sup>45,46</sup> proposed his initial model function:  $N(dM) \propto M^\alpha$ , where  $N(dM)$  is the number of stars in the mass range  $M$  to  $M+dM$  per  $\text{pc}^3$ . Detailed analysis of the different models has been provided by Bolzonella et al<sup>47</sup>, who

opted for the model of Miller and Scalo<sup>48</sup>, with a 4-part segmentation of alpha for  $M$  ranging from  $0.1 - 100M_{\odot}$ . Because of the rapid decline in number counts of more massive stars in this model, 52% of the mass resides in stars with a mass  $\leq 1 M_{\odot}$ , and 91% of the mass is in stars with a mass  $\leq 10 M_{\odot}$ .

Applying an IMF function to the mass distribution of the dynamic model of Section 4 with equipartition of energy among the mass components will change the characteristics of the density, radius and velocity profiles. There is an increase in core density and a more rapid reduction in shell density with radius; the core velocity is decreased slightly, whilst the final galactic radius is increased by the faster moving low mass components. Although the exact profiles are IMF dependent, the overall picture is reasonably well described by the simpler analysis using a single mean stellar mass value.

#### 4.4. The core of globular clusters

There has been much debate about the possible existence of a black hole at the centre of GCs (e.g. Gerssen et al<sup>49</sup>). However, theoretical models suggest that a GC does not require a black hole core. A number of mechanisms account for a paucity of massive stars in GCs: (1) the initial number of massive stars (i.e.  $> 10 M_{\odot}$ ) was probably low as a statistical consequence of the GCs being small systems with few stars; (2) the age of GCs implies that no early stars with initial mass  $> 2.5 M_{\odot}$  will still be present in a small GC, as they will have formed supernovae shortly after the formation of the GC; (3) the low mass of GCs may have prevented the retention of secondary elements formed by the early supernovae, and hence any consequent population I secondary star formation will have been suppressed; (4) and conversely stars with very low mass ( $\approx 0.1 M_{\odot}$ ) may not have ignited, and possibly were sling shot out of their parent GC.

Assuming a total stellar mass of  $4.5 \times 10^5$  and radius of 25pc for M15, the present analysis suggests that the mean distance between stars in the core of even a large GC such as M15, is  $\sim 1.5 \times 10^{12}$ m, and will occupy a volume of  $\sim 1.5 \times 10^{37}$ m<sup>3</sup>. The volume of a star of stellar mass is  $\sim 1.4 \times 10^{27}$ m<sup>3</sup>, i.e. there is a volume ratio of  $1.09 \times 10^{10}$  which implies a very low probability for core stars to coalesce to form a new black hole.

## 5. CROSS-SECTIONAL DENSITY

### 5.1. Sphere with uniform density

Emission profiles of galaxies map surface luminosity per unit area as a function of galactic radius. These profiles are clearly dependent on mass/luminosity function, and the obscuring of deeper stars by dust. Without going into this level of detail, it is interesting to look at the number of stars per unit area as a function of radius. For a galaxy of uniform density  $\rho_f$ , and radius  $r_f$ , this is of course a trivial question:

$$N(r) = 2\rho_f \sqrt{r_f^2 - r^2} \quad (5.1.1)$$

where  $N(r)$  is the number density of stars observed per unit area.

### 5.2. Sphere with density increasing towards the centre

A more realistic relationship for globular clusters (GC) with density increasing towards the centre was initially described by King<sup>50</sup>. He presented an empirical formula that represented the density from centre to edge in globular clusters of the form:



$$\therefore N(r) = 2\rho_f \Delta A \int_0^L \frac{r_f^2}{r^2 + l^2} dl = 2\rho_f \Delta A \frac{r_f^2}{r} |\tan^{-1}(l/r)|_0^L \quad (5.2.3)$$

i. e. 
$$N(r) = 2\rho_f \Delta A \frac{r_f^2}{r} \left[ \tan^{-1} \left( \frac{r_f^2}{r^2} - 1 \right)^{1/2} \right] \quad (5.2.4)$$

Note that  $N(r) \rightarrow 0$  for  $r \rightarrow r_f$ , while for the limit  $r \ll r_f$ , this simplifies to:

$$N(r) \cong \frac{\pi\rho_f \Delta A r_f^2}{r} \quad (5.2.5)$$

which is a simple power curve with log-log slope -1. The implied limit  $N(r) \rightarrow \infty$  as  $r \rightarrow 0$  is not a physical reality; in practice, observed stars have a finite resolvable disk, whose diameter is set by the resolving power of the telescope. In addition, it may be assumed that the star number density cannot increase beyond a certain limiting threshold, beyond which individual stars may conjoin, possibly as a central black hole. This sets an upper bound to the number of stars that can be distinguished in any given star field. If we define this radius to be  $r_c$ , this represents a lower bound for  $r$  in (5.2.4), from which we may generate the limiting curve:

$$N(r) = 2\rho_f \Delta A \frac{r_f^2}{(r + r_c)} \left[ \tan^{-1} \left( \frac{r_f^2}{(r + r_c)^2} - 1 \right)^{1/2} \right] \quad (5.2.6)$$

Such a curve has only three parameters:  $\rho_f$ ,  $r_f$ , and  $r_c$ , and superficially resembles that of King, but it differs in concept, and in the detail of its shape. Whereas King's curves were constructed *ad hoc* to fit the observational data, the curve described in (5.2.6) was generated from a model of the behaviour of stars in a relaxed spherical galaxy.

### 5.3. Limitations of the model

In common with King's equations, Equation 4.6 assumes a definite maximum radius,  $r_f$ , a limiting edge density  $\rho_f$ , and a defined core radius,  $r_c$ . Implicit also is the assumption that kinetic energy is partitioned equally within each shell, and that all stars have identical masses. This latter is the least plausible assumption, and a better model might be created using an idealised initial mass function (IMF) such as that of Salpeter. This presents an empirical IMF  $P(n) \propto m^{-2.35} \propto r^{-7.05}$ , where  $P(n)$  is the probability of observing  $n$  stars of given mass  $m$ .

Figure 38 represents the simulated field of view of a plate 2x2 arc minutes, with a true star density of 100 stars per square arc min. Unobscured stars are shown in green; the yellow stars represent an overlap of the optical disks, with the degree of overlap ranging from brushing edges to complete masking, and this clearly affects the final counts. The stars outside the plate area are included to allow for completeness in the algorithm for assessing visible star counts. It may be seen that a majority of star disks show some degree of overlap. By pixel counting in the plate area, an estimate may be drawn for the degree of overlap for any given star density and distribution of apparent radii.

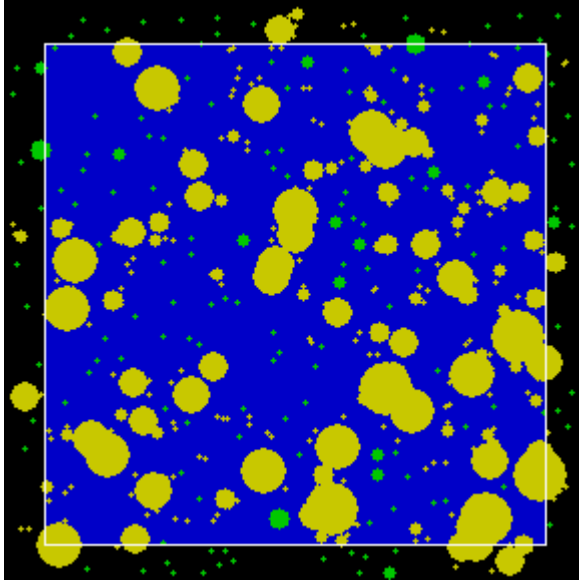


**Figure 38. Simulated star field for star count corrections**

The formal analysis of the equations of motion for stars of differing masses within globular clusters is complex, but by using an IMF of simplified Salpeter form such as  $P(n) \propto m^{-2}$  one may derive a modified function for the predicted number counts (5.3.1).

$$N(r) = \rho_f \left( \frac{r_f^4 + 2r_f^2(r + r_c)^2}{3(r + r_c)^4} \right) \sqrt{r_f^2 - (r + r_c)^2} \quad (5.3.1)$$

Figure 39 and Figure 40 show two plots using this curve, with parameters adjusted for best fit to observational data for the globular clusters NGC 5053 and M15.

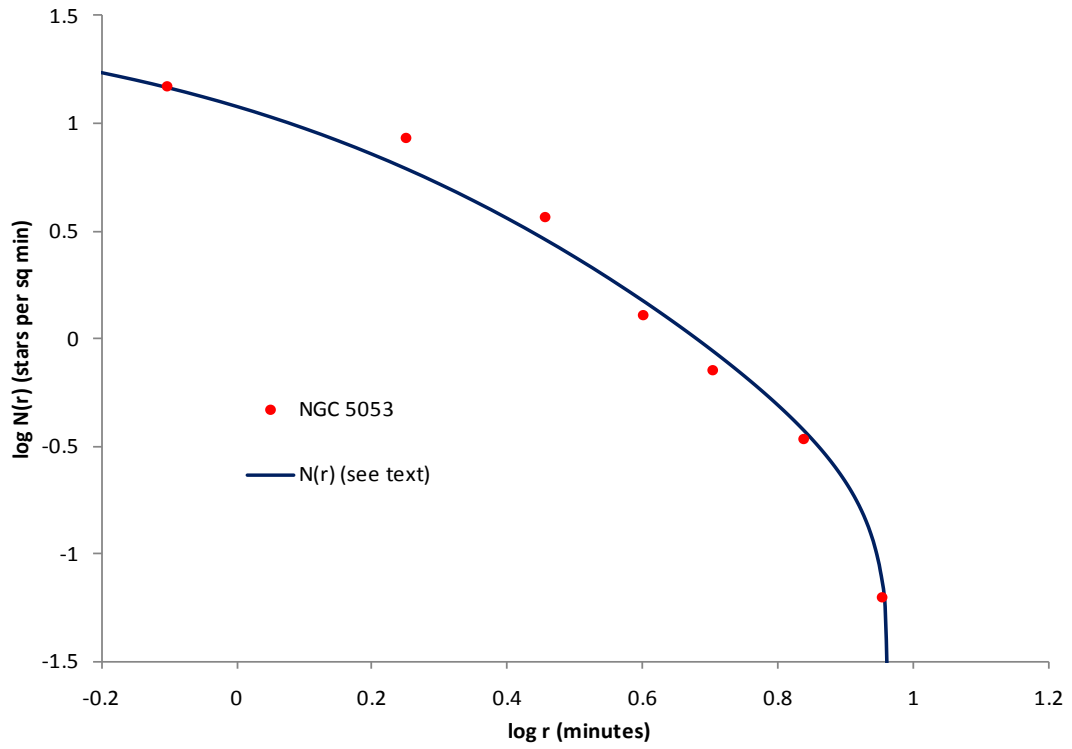


Figure 39. NGC5053 data vs  $N(r)^{50}$

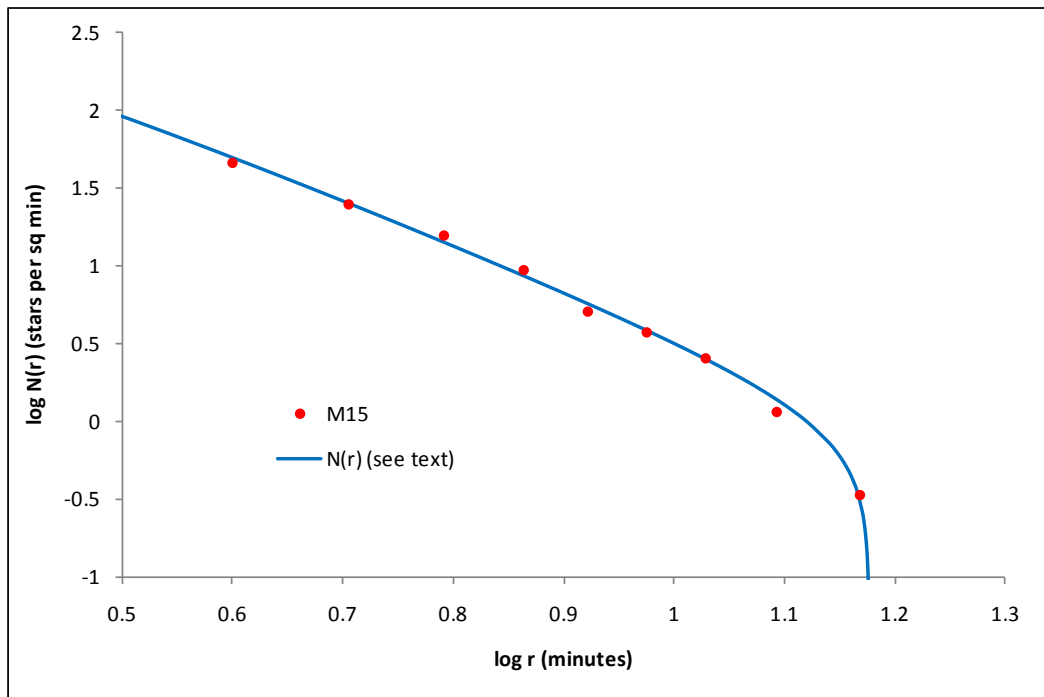


Figure 40. M15 data vs  $N(r)^{50}$

## 6. DISCUSSION

The early epochs of the universe are now well understood in terms of nucleosynthesis, and the partition of energy up to the epoch of decoupling, when hydrogen ions became neutral and transparent to light. With the increasing sensitivity of COBE and the Wilkinson Microwave Anisotropy Probe (WMAP) satellite project<sup>51</sup>, finer details of the anisotropies in the background radiation are becoming apparent, and give hints of early structure and consequent galactic separation, possibly through the amplification of quantum fluctuations within the proto-universe itself.

The analyses of a number of self-gravitational systems are presented in this paper, using solely Newtonian dynamics. By using the technique of numerical integration, accurate rotation curves can be derived for any given distribution of bulge or disk density. The computer models were run using only Newtonian gravity interacting between stars within the disks to examine the velocity curves for a number of different density profiles. It is shown that, far from producing a simple Newtonian decay curve, the stable rotational velocity of a thin disk is highly sensitive to the surface density/mass distribution for the disk. By looking at a number of density profiles, a wide variation in rotational curves can be generated, including flat curves. The models are fitted to observational data for a range of galaxy types, including low surface brightness, dense compact galaxies, and bright spirals such as M31. Using only the bulge mass and a disk density distribution with a truncated disk boundary, it is demonstrated that a number of galaxy rotation curves can be fitted well without recourse to DM halos or MOND.

Three distinct types of velocity curves are generated in these models. In Type 1 curves, the velocity continues to rise with increasing  $r$ ; this is typically associated with a relatively uniform disk mass/density distribution. Type 2 curves rise to a maximum, before declining as the radius increases; these may be associated with a mass/density distribution tapering towards zero. Type 3 curves rise to a plateau which may be flat, but then show a characteristic terminal increase in velocity; these curves are associated with a decreasing disk mass/density which truncates at its terminus. These curves are in broad agreement with Verheijen's classification of 'R', 'D' and 'F' type curves respectively<sup>19</sup>. Of specific interest are curves with a finite (i.e. truncated) inverse- $r$  mass/density distribution; these curves are remarkably flat over most of the observational radius, but terminate with an increase in rotational velocity. The density distributions used in the models conform well to a number of surface brightness observations, and these curves can be shown to predict a Tully-Fisher relationship.

Although it might be anticipated that a Newtonian decay will occur at sufficiently remote distances from the galactic centre, it is postulated that such curves will not be seen, because the presence of any observational mass does not have a neutral effect, but does itself have a profound influence on the shape of the curves. A number of previous papers have demonstrated analytically derived rotation curves for axially symmetric disks with an exponential or an inverse- $r$  density function, but these have generally been for well-defined models with an infinite maximum radius. Analytical models for other density distributions and finite radii are difficult to implement.

A brief consideration of statistical thermodynamics suggests that a galaxy with angular momentum will attain a stable disk equivalent to an adiabatic thermodynamic system in thermal equilibrium with equipartition of kinetic energy across the resultant disk (a micro

canonical ensemble). Such a system implies an inverse- $r$  mass/density distribution, with uniform velocity. A dynamic model is also presented which can be shown to evolve towards stability by attaining a flattened velocity curve, with a truncated disk approximating an inverse- $r$  mass/density distribution.

Whatever the mechanism for the formation of individual galaxies, it is generally accepted that they must have condensed out of a medium that was, at least initially, approximately homogenous. Gravitational instability then acted upon minor perturbations within this medium, allowed the separation of individual pro-galactic units that went on to collapse through their own self gravity against the background of an expanding universe. This allowed the mean separation of galactic centres to continue to increase, even as the galaxies themselves contracted in size. Modelling globular clusters without overall angular momentum suggests that they attain a stable final radius, with a predicted density and velocity distribution that match observational data reasonably well, and it is demonstrated that the ratio of mean separation distance:galactic radius is a constant for a given epoch, with a plausible present day value, without requiring DM halos or modification to Newtonian gravitation. These models do not preclude the existence of DM in GCs, but they do suggest that the distribution of any DM follows the distribution of the observed stellar masses.

A number of theoretical predictions suggest the existence of DM to make up missing mass from the universe, and within galaxies. It is not the purpose of this paper to consider missing dark mass candidates or their detailed behaviour; however, it is proposed that any DM candidate particles will be gravitationally bound by their own galaxy or GC. Within a GC, such particles will behave as the ‘particles’ of the star systems, i.e. they will exchange PE for KE as they move towards the centre under gravity, and they will gravitationally react with other particles to exchange momentum in an elastic manner to reach thermal equilibrium.

Casertano<sup>22</sup> has described the relationship between DM and baryonic matter as a conspiracy theory to produce flat rotation curves; similarly, Swaters<sup>52</sup> has shown that, for a number of observations, rotation curves can be fitted equally between minimum and maximum disk mass models, and almost anything between. In a disk galaxy, DM particles too may be assumed to have angular momentum, acquired in the same manner and at the same time as the baryonic matter. DM may therefore be predicted to also move in a flattened disk, and ought to share the gravitational characteristics and mass distribution of the visible disk. The models presented here do not preclude the presence of DM from the disks; however, as with the GC models, the DM should be confined within the disk to add to the observed baryonic mass to obtain the observed curves. Because the modelled curves mimic the observational data so closely using standard Newtonian self-gravitational models, it is proposed that undetectable DM halos are not required, and the invocation of an *ad hoc* adjustment to Newtonian gravitation as proposed by MOND becomes superfluous.

Whilst it is recognised that these Newtonian models will be controversial, nevertheless it is considered that a model that gives a reasonable fit to observations, without recourse to unobserved physical parameters, is worth considering. To paraphrase Hubble: “...it is still premature to base conclusions on these [variables in] spirals, but the straws are all pointing on one direction and it will do no harm to begin considering the various possibilities involved<sup>53</sup>”; and “we cannot assume that our knowledge of physical principles is yet complete; nevertheless, we should not replace a known, familiar principle, by an *ad hoc* explanation unless we are forced to that step by actual

observations.”<sup>54</sup> Perhaps now it is time to consider the possibility that the dynamics of spirals conform to standard Newtonian gravitation, without recourse to MOND or DM halos.

## 7. REFERENCES

- 
- <sup>1</sup> Milgrom, M. A modification of the Newtonian dynamics as a possible alternative to the hidden mass hypothesis. 1983, *ApJ*, 270, 365
- <sup>2</sup> Sanders RH. The published extended rotation curves of spiral galaxies: Confrontation with Modified Dynamics. *Astrophysics* 1999. <http://arxiv.org/abs/astro-ph/9606089v1>.
- <sup>3</sup> Sanders RH, McGaugh SS. Modified Newtonian Dynamics as an Alternative to Dark Matter. *Annual Review of Astronomy and Astrophysics* 2002; 40: 263-317.
- <sup>4</sup> Swaters RA, Sanders RH, Mcgaugh SS. Testing Modified Newtonian Dynamics with Rotation Curves of Dwarf and Low Surface Brightness Galaxies. *ApJ* 2010; 718: 380-391. arXiv:1005.5456v1 [astro-ph.CO]
- <sup>5</sup> de Blok WJG, McGaugh SS. Testing Modified Newtonian Dynamics With Low Surface Brightness Galaxies: Rotation Curve Fits. *The Astrophysical Journal* 1998; 508:132-140.
- <sup>6</sup> Brownstein JR, Moffat JW. Galaxy Rotation Curves without Nonbaryonic Dark Matter. *The Astrophysical Journal* 2006; 636:721-741.
- <sup>7</sup> Balasin H, Grumiller D. DFG project GR-3157-1/1 2006; Institute for Theoretical Physics, University of Leipzig.
- <sup>8</sup> Fabris JC, Pereira Campos J. Spiral galaxies rotation curves with a logarithmic corrected Newtonian gravitational potential. *Gen Relativ Gravit* 2009; 41:93–104.
- <sup>9</sup> Eckhardt DH, Pestaña JLG. Technique for Modeling the Gravitational Field of a Galactic Disk. *AJ* 2002; 572:L135–L137.
- <sup>10</sup> Nicholson KF. Galaxy mass distributions from rotation speeds by closed-loop convergence. arXiv 2003; astro-ph/0303135.
- <sup>11</sup> Banhatti DG. Newtonian mechanics and gravity fully model disk galaxy rotation curves without dark matter. *IAU Symposium 254 on Galaxy Disk in Cosmological Context*, 9-14 June 2008, Copenhagen, Denmark.
- <sup>12</sup> Kochanek CS. Rapid Calculation of Equatorial Rotation Curves. 2008; astro-ph/0108162v1.
- <sup>13</sup> Keepports D. Mass Distributions Implying Flat Galactic Rotation Curves. *2010 Eur J Phys* 2010; 31: 519.
- <sup>14</sup> Toomre A. On the Distribution of Matter within Highly Flattened Galaxies. *ApJ* 1963; 138: 385-392.
- <sup>15</sup> Freeman KC. On the Disks of Spiral and S0 Galaxies. *ApJ* 1970; 160: 811.
- <sup>16</sup> Kent, S. M. Dark matter in spiral galaxies. I - Galaxies with optical rotation curves. *AJ* 1986; 91: 1301.
- <sup>17</sup> Cuddeford P. On the potentials of galactic disks. *MNRAS* 1993; 262: 1076-1086.
- <sup>18</sup> Conway JT. Analytical solutions for the Newtonian gravitational field induced by matter within axisymmetric boundaries *MNRAS* 2000; 316: 540-554.
- <sup>19</sup> Verheijen MAW. The Ursa Major Cluster of Galaxies. V; HI Rotation Curve Shapes and the Tully-Fisher Relations. 2001; astro-ph/0108225v1.
- <sup>20</sup> Dalziel S. *Numerical Methods*. Dep Ap Math and Theoretical Phys, U of Cambridge. 1998.
- <sup>21</sup> Carignan C, Purton C. The Total Mass of DDO 154. *AJ* 1998; 506:125–134.
- <sup>22</sup> Casertano S, van Gorkom JH. Declining Rotation Curves: The End of a Conspiracy? *AJ* 1991; 101: 1231-1241.
- <sup>23</sup> Peacock, JA. The galaxy population. in *Cosmological Physics*: p387-9. Camb UP. 1999.
- <sup>24</sup> de Vaucouleurs G. Photoelectric photometry of the Andromeda nebula in the UBV system . *ApJ* 1958; 128: 465.

- 
- <sup>25</sup> Takase B. Distribution of Mass, Angular Momentum, and Rotational Energy in the Galaxy and NGC 224. *Pub Astr Soc Japan* 1967; 19: 427.
- <sup>26</sup> Mestel L. On the galactic law of rotation. *MNRAS* 1963; 126: 553.
- <sup>27</sup> Meurer GR. The Dark Blue Compact Dwarf Galaxy NGC2915. *PASAu* 1997; 14: 77-80.
- <sup>28</sup> Elson EC, de Blok WJG, Kraan-Korteweg RC. The dark matter content of the blue compact dwarf NGC 2915. *MNRAS* 2010 (2 Feb); e-print.
- <sup>29</sup> Carignan C, Chemin L, Huchtmeier WK, Lockman FJ. Extended HI Rotation Curve and Mass Distribution of M31. *ApJ* 2006; 641: L109.
- <sup>30</sup> Rubin VC, Kent Ford W. Rotation of the Andromeda Nebula from a Spectroscopic Survey of Emission Regions. *ApJ* 1970; 159: 379-403.
- <sup>31</sup> Afanasiev VL, Silichenko OK. Global Structure and Kinematics of the Spiral Galaxy NGC 2841. *Astro J* 1999; 117:1725-1732.
- <sup>32</sup> Bottema R, Pestaña JLG, Rothberg B, Sanders RH. MOND rotation curves for spiral galaxies with Cepheid-based distances. *A&A* 2002; 393: 453-460.
- <sup>33</sup> de Blok WJG, McGaugh SS, van der Hulst JM. HI observations of low surface brightness galaxies: Probing low-density galaxies. *MNRAS* 1996; 283: 18-54.
- <sup>34</sup> Swaters RA, Madore BF, Trewella M. High-Resolution Rotation Curves of Low Surface Brightness Galaxies. *The Astrophysical Journal* 2000; 531:L107-L110.
- <sup>35</sup> Tully RB, Fisher JR. A New Method of Determining Distances to Galaxies. *Astron Astrophys* 1977; 54: 661-673.
- <sup>36</sup> van der Kruit PC, Searle L. Surface photometry of edge-on spiral galaxies. *Astron Astrophys* 1981; 95: 105-115.
- <sup>37</sup> Bizyaev DV, Zasov AV. Disk Boundaries in Spiral Galaxies. *Astronomy Reports* 2002; 46 (9): 721-730.
- <sup>38</sup> Singhal A. The Connection between Galaxy Kinematics and HI Line Widths as Applied to the Distance Scale. PhD Dissertation, Department of Astronomy, University of Virginia. 2008.
- <sup>39</sup> Griv E, Gedalin M. Changes of Angular Momentum and Entropy Induced by Jeans-Unstable Density Waves in Stellar Disks of Flat Galaxies. *AJ* 2004; 128:1965-1973.
- <sup>40</sup> Wolfram Mathematica, Standard integrals. <http://integrals.wolfram.com/index.jsp>.
- <sup>41</sup> Lehnert MD, Nesvadba NPH, Cuby J-G, et al. Spectroscopic confirmation of a galaxy at redshift  $z = 8.6$ . *Nature* 2010 (Letter 21 Oct); 467: 940-942. doi:10.1038/nature09462. Published online 20 Oct 2010.
- <sup>42</sup> Komatsu E, Dunkley J, Nolte MR, et al. Five-Year Wilkinson Microwave Anisotropy Probe Observations: Cosmological Interpretation. *ApJS* 2009; 180 (2): 330. doi:10.1088/0067-0049/180/2/330.
- <sup>43</sup> Menegoni e, et al. New constraints on variations of the fine structure constant from CMB anisotropies. *PhysRevD* 2009; 80 (8): 087302. arXiv:0909.3584. doi:10.1103
- <sup>44</sup> McNamara BJ, Harrison TE, Baumgardt H. The dynamical distance to M15: estimates of the cluster's age and mass and of the absolute magnitude of its RR Lyrae stars. *Astrophys J.* 2004; 602:264-270.
- <sup>45</sup> Salpeter EE. The Luminosity Function and Stellar Evolution. *ApJ.* 1955; 121: 161.
- <sup>46</sup> Chabrier G. The Initial Mass Function : From Salpeter 1955 to 2005. 20 Sep 2004. arXiv:astro-ph/0409465v1.
- <sup>47</sup> Bolzonella M, Miralles J -M, Pelló R. Photometric redshifts based on standard SED fitting procedures. *Astron. Astrophys* 2000; 363: 476-492.
- <sup>48</sup> Miller GE, Scalo J M. The initial mass function and stellar birthrate in the solar neighbourhood. *ApJS* 1979; 41: 513.
- <sup>49</sup> Gerssen J, van der Marel RP, Gebhardt K, et al. Hubble Space Telescope Evidence for an Intermediate-Mass Black Hole in the Globular Cluster M15. II. Kinematic Analysis and Dynamical Modeling. *AJ* 2002; 124: 3270.
- <sup>50</sup> King, I. The structure of star clusters. I. An empirical density law. *AJ* 1962; 67:471-85.

---

<sup>51</sup> Hinshaw G. et al. Five-Year Wilkinson Microwave Anisotropy Probe (WMAP) Observations: Data Processing, Sky Maps, and Basic Results. *Astrophysical Journal Supplement* 2009; 180: 225-245.

<sup>52</sup> Swaters RA. The Mass Distribution in Low Surface Brightness Galaxies. in: *Galaxy Disks and Disk Galaxies*, proceeding of a conference held in Rome, Italy, June 12-16 2000. *ASP Conference Series*, Vol. 230. Ed: Funes JG, Corsini SJ and EM: 545-548. 2001.

<sup>53</sup> HUA Hubble to Shapley, August 25, 1924.

<sup>54</sup> Hubble E. *The Observational Approach to Cosmology*. Oxford: Clarendon Press; p.26. 1937.